buildings

MDPI

Article

Climatic Adaptability of Transitional Space in Traditional Courtyard Dwellings of Jinhua: A Case Study of the Lu Residence in Dongyang

Jiaqi Wang [1], Huijie Liu [1] and Li Bao [2,*]

[1] Zhejiang Province Institute of Architectural Design and Research Co., Ltd., Hangzhou 310006, China; kaetc312@outlook.com (J.W.); liuhuijie2025@outlook.com (H.L.)
[2] School of Architecture, Southeast University, Nanjing 210096, China
* Correspondence: baoli@seu.edu.cn

Abstract

Amid the combined pressures of global carbon-reduction in architecture and the imperative of cultural heritage conservation, new courtyard-style buildings in hot-summer and cold-winter regions face a dual challenge of reconciling historical morphological constraints with contemporary comfort requirements. At the same time, the prevailing energy-efficiency codes in these regions, emphasizing high airtightness and strong insulation, have revealed shortcomings such as poor indoor air quality and insufficient summer ventilation. This study takes the Lu Residence in Dongyang, Jinhua, Zhejiang Province, as the primary case. It systematically examines the coupling mechanisms between the geometric configurations of transitional space in traditional courtyard dwellings and their environmental physical parameters using field surveys, multi-parameter environmental monitoring, and computer simulations. The results identify the optimal orientations and geometric parameters that balance summer ventilation with winter thermal buffering in hot-summer and cold-winter regions. The primary conclusions of this research are as follows: (1) The optimal orientation for axial buildings lies between 15° west of south and 15° east of south, as well as 30–60° east or west of south, with an angle of 45–60° in relation to the prevailing annual wind direction for all buildings. (2) The optimal height-to-width ratio of the courtyard is less than 1:2.5, while the range of the length-to-width ratio extends from 1:0.5 to 1:0.7. (3) The optimal eave depth varies from 900 to 1500 mm, effectively balancing winter heat retention and summer shading; however, a depth of 2400 mm is primarily advantageous for shading purposes. Furthermore, these findings are applied to the design of a new guesthouse within the conservation area of the Xu Zhen Er Gong Ancestral Hall in Yongkang, establishing a climate–geometry matching mechanism for transitional spaces. The study demonstrates that transitional space can serve as effective passive regulators, offering a scientific and sustainable pathway for the adaptive continuation of traditional courtyard architecture.

Keywords: traditional courtyard dwellings; transitional space; environmental adaptability; passive climate control; hot-summer and cold-winter climate; Lu residence

check for updates

Academic Editor: Alireza Afshari

Received: 30 September 2025
Revised: 26 October 2025
Accepted: 29 October 2025
Published: 5 November 2025

Citation: Wang, J.; Liu, H.; Bao, L. Climatic Adaptability of Transitional Space in Traditional Courtyard Dwellings of Jinhua: A Case Study of the Lu Residence in Dongyang. *Buildings* **2025**, *15*, 3999. https://doi.org/10.3390/buildings15213999

Copyright: © 2025 by the authors. Licensee MDPI, Basel, Switzerland. This article is an open access article distributed under the terms and conditions of the Creative Commons Attribution (CC BY) license (https://creativecommons.org/licenses/by/4.0/).

1. Introduction

Green architecture has emerged as a prominent subject within contemporary architectural discourse and represents a strategic priority in national development initiatives. The examination of green buildings encompasses not only technological methodologies

to address climatic and environmental challenges but also emphasizes the importance of cultural, historical, and socio-economic contexts that influence the built environment. As recognition of the significance of traditional architecture increases, the conservation of historic structures and the perpetuation of cultural heritage have garnered widespread consensus within both architectural practice and urban renewal efforts. Consequently, the integration of traditional wisdom into modern design, while maintaining contemporary standards of climatic comfort, has become an essential challenge confronting architects engaged in works within historic environments.

The traditional philosophy of harmony and adaptation in vernacular dwellings reflects the ancient people's intuitive understanding of and effective response to their environment. It also embodies the humanistic and technical concerns central to green architecture. In the Jinhua region, a distinctive characteristic of courtyard dwellings is the inclusion of a significant proportion of semi-outdoor spaces—such as courtyards, eave galleries, and passage halls—that connect indoor and outdoor areas and possess incomplete climatic boundaries. These are defined in this study as transitional spaces. Similar to interior rooms, transitional spaces serve as primary venues for daily life in courtyard dwellings.

Unlike contemporary energy-efficient design approaches [1] that emphasize sealed envelopes, transitional spaces in traditional dwellings regulate the thermal environment through airflow organization, radiative modulation, and thermal buffering in a non-sealed manner. The key questions this study addresses are: how these transitional spaces respond to the hot-summer and cold-winter climatic conditions of Jinhua, and to what extent their passive regulation strategies contribute to achieving a livable thermal environment.

Traditional vernacular dwellings have long been a central subject of research in Chinese architecture. Initial investigations predominantly concentrated on the material aspects of dwellings, analyzing components such as floor plans, structural frameworks, and decorative elements, thereby developing a typological framework for traditional residences [2–6]. Recently, with the escalating importance of environmental conservation, green architecture has emerged as a significant issue within the discipline, and the ecological wisdom inherent in traditional buildings has garnered heightened acknowledgment.

As essential spatial components of traditional Chinese architecture, courtyards and patios have been extensively studied in terms of their contributions to environmental comfort [7–16]. Chen [17] investigated the regional adaptability of Xiguan Grand House from the perspectives of natural, social, and cultural adaptation; Pan [18] constructed three-dimensional models and employed computer simulations to explore the influence of patio geometry on the wind environment in Huizhou dwellings; Hao [19] demonstrated through field measurements that patios can significantly reduce daytime peak air temperatures; Chen [20] focused on the mechanisms of thermal regulation in patios, optimizing orientation, height, and aspect ratio parameters. Furthermore, numerous studies have shown that courtyards play an important role in climatic regulation in contemporary architecture worldwide, and optimization strategies have been proposed at multiple scales. Rodriguez-Algeciras [21] identified the significant effect of courtyard height-to-width ratio on thermal performance through modeling; Fabbri [22] examined the impact of different shading devices on outdoor courtyard thermal comfort; Abdallah [23] combined field monitoring with parametric simulations to propose optimization strategies for campus environments in Egypt. Collectively, these studies have not only deepened the understanding of environmental regulation mechanisms in traditional architecture but also provided prototype languages for contemporary design.

Computational simulation, as an indispensable instrument for analyzing wind and thermal conditions, has been extensively utilized in evaluating building environmental performance and supporting architectural design [24–27]. Liu [28] assessed outdoor

wind comfort and proposed optimization strategies through field measurements and CFD simulations in the Maritime Silk Road heritage sites in Quanzhou; Zhao [29] examined the positive effects of Feng Shui–based layouts on courtyard wind environments, using Bailudong Academy as a case study; Liu [30] investigated spatial configurations, building morphologies, and facility strategies to maximize solar energy utilization in cold-climate regions through monitoring and simulation; Wan [31] derived prototypes of wind-driven and buoyancy-assisted ventilation from traditional Chaoshan villages and applied these to the design of visitor centers. These studies illustrate that computational simulation effectively elucidates the interaction mechanisms between spatial form and environmental performance in both traditional and contemporary structures, thereby providing a scientific foundation for spatial optimization.

Nevertheless, current research continues to reveal limitations concerning transitional spaces in traditional courtyard residences located in regions characterized by hot summers and cold winters.

- Gaps in the understanding of spatial hierarchy: while most research concentrates on the two scales of "settlement–indoor," transitional spaces—distinguished by their distinctive role in mediating between outdoor and indoor climates—continue to be inadequately quantified.
- The deficiency of winter–summer synergy: prior research frequently emphasizes a singular objective, either summer ventilation or winter insulation. However, regions experiencing hot summers and cold winters necessitate a dual-mode strategy of "winter sheltering and summer ventilation," which remains insufficiently explored.
- Limited parameter integration: the majority of studies address either wind or thermal environments in isolation. However, comfort necessitates the synergistic interaction of wind, light, and heat.

In summary, research on environmental comfort in traditional architecture has evolved from single-variable performance analysis to a comprehensive stage characterized by multi-system coupling and multi-objective optimization. Through field investigations and computational simulations, this study systematically quantifies the role of transitional spaces in the winter wind–light–heat synergistic regulation of courtyard dwellings. It further proposes optimal geometric parameters for orientation, courtyard configuration, and eave depth, as well as green design strategies at the cluster level. These findings are applied to the practical design of newly built traditional-style architectures in the region, providing a feasible and applicable design approach for similar construction contexts.

2. Research Objects and Methods

2.1. Regional Context

2.1.1. Jinhua Region

The Jinhua region is located in the eastern part of the Jinqu Basin within central Zhejiang Province. It is characterized by a subtropical monsoon climate with basin climate features, influenced by the East Asian monsoon system. During winter, cold and dry northwesterly monsoons predominate, whereas in summer, warm and humid southeasterly monsoons are prevalent. The average annual temperature is 18.1 °C, with January averaging 5.7 °C and July reaching 29.7 °C. Annually, the region receives approximately 1493 mm of rainfall across about 155 rainy days. During the plum rain season (April to June), more than 40% of the annual precipitation occurs, establishing a characteristic monsoon pattern described as "humid spring, hot summer, dry autumn, and cold winter." According to the Thermal Design Code for Civil Buildings (GB 50176-2016) [32], Jinhua is classified within a "hot-summer and cold-winter" region, subregion 3B. Therefore, considerations of thermal

insulation and heat retention are paramount, with an emphasis on natural ventilation and shading.

Due to the surrounding mountains flanking both sides of the basin, the prevailing wind patterns in Jinhua are significantly influenced by the terrain and exhibit minimal seasonal variation. Generally, the primary wind directions remain consistent on an annual basis, although they vary among different locations: in Jinhua, the predominant wind is from the east-northeast; in Lanxi and Yongkang, from the north-northeast; in Wuyi, from the north and north-northeast; in Pujiang, from the east and east-southeast; in Yiwu, from the north; and in Dongyang, from the northwest [33].

Research on interannual climate variation [34] indicates that the Jinhua region experienced a significant warming trend during 1968–2019, with an average annual temperature increase of approximately 0.04 °C per year under the climatic normal. Across different periods, the rate of warming was slightly lower during 1971–2000 (0.01 °C/year below the normal), accelerated during 1981–2010 (0.02 °C/year above the normal), and was comparable to the normal during 1990–2019 (Figure 1a). The sunshine duration demonstrated a notable decreasing trend, with an average reduction of approximately 8.0 h annually. Among various periods, sunshine duration was marginally higher during 1971–2000 (4.2 h/year above the overall mean), whereas it was reduced during 1981–2010 and 1990–2019 (by 4.2 h/year and 2.9 h/year below the overall mean, respectively) (Figure 1b). Under different climatic normals, the central region of Jinhua consistently exhibits higher temperatures compared to the northern and southern regions, displaying a spatial pattern characterized by "low in the north and south, high in the center" (Figure 1c). This pattern indicates that, during summer, buildings generally necessitate enhanced shading measures and optimized passive ventilation to facilitate cooling. Although the overall climate in Jinhua shows a warming trend, winter thermal comfort remains dependent on building heat gains under various climatic normals. The central and northern areas, which receive more sunlight (Figure 1d), should ensure south-facing daylight access and reduce winter shading. Conversely, the western and southern regions receive less sunshine, thereby requiring adjustments in building orientation, window transmittance, and improved insulation to mitigate occasional low temperatures.

2.1.2. Representative Traditional Vernacular Dwellings of the Region

A considerable number of Ming dynasty dwellings are still preserved in the Jinhua region, typically comprising residential compounds of the gentry consisting of thirteen interconnected rooms, commonly referred to as "dahurenjia" (grand residential compound) or colloquially as "Shisan jiantou" (Thirteen-Bay House) [35]. The Thirteen-Bay House accommodates three generations of a family living together around a shared hearth. The basic structure extended longitudinally into multiple courtyards and laterally into expansive complexes that housed brothers and uncles. When constructed in both directions, these formations created large complexes capable of sheltering an entire clan. As these compounds increased in number, villages expanded into towns, which subsequently developed into small cities. This evolution contributed to the emergence of a distinctive architectural style in the Jinhua region, known as "Wupai jianzhu" (Wu-style architecture). Fundamentally, the "Thirteen-Bay House" served as the foundational unit and core of this architectural tradition. The basic information regarding the Thirteen-Bay House is provided below.

- Origin: Following the southward migration of the Song imperial court, northern literati established settlements across the counties of Jinhua. Dwellings were constructed in compliance with state-sanctioned hierarchical codes and the imperial construction manual *Yingzao Fashi*.
- Entrance Position: Center of the main façade wall.
- Building Height: One or two stories.

- Courtyard Combination Patterns: "Shiba jiantou" (Eighteen-Bay House) adds five inverted rooms opposite the main hall, one serving as the entrance hall, forming a "hui" -shaped lan. "Ershisi jian" (Twenty-Four-Bay House) merges two Thirteen-Bay Houses longitudinally, featuring a triple courtyard at the front and a quadruple courtyard at the rear, thereby forming a "ri"-shaped plan.
- Plan Layout: The junction between the main hall and side wings is connected by "dongtou houses" (flanking rooms) and "nongtang" (connecting gallery).
- Single-Building Form: The main hall and both wings each comprise three bays. The symmetrical façade features a central, elevated main hall, flanked by slightly lower gable walls and courtyard walls, creating a "three-high, one-low" configuration.
- Structural System: A through-purlin (chuandou) timber frame or a hybrid structure comprising the central bay in the post-and-beam (tailiang) system and the side bays in the through-purlin system.
- Roof Type: Gabled roofs, some with two-story double eaves.
- Envelope Materials: Stone foundations with rammed earth or brick walls above.
- Doors and Windows: Lattice panels often decorated with carved ornaments.

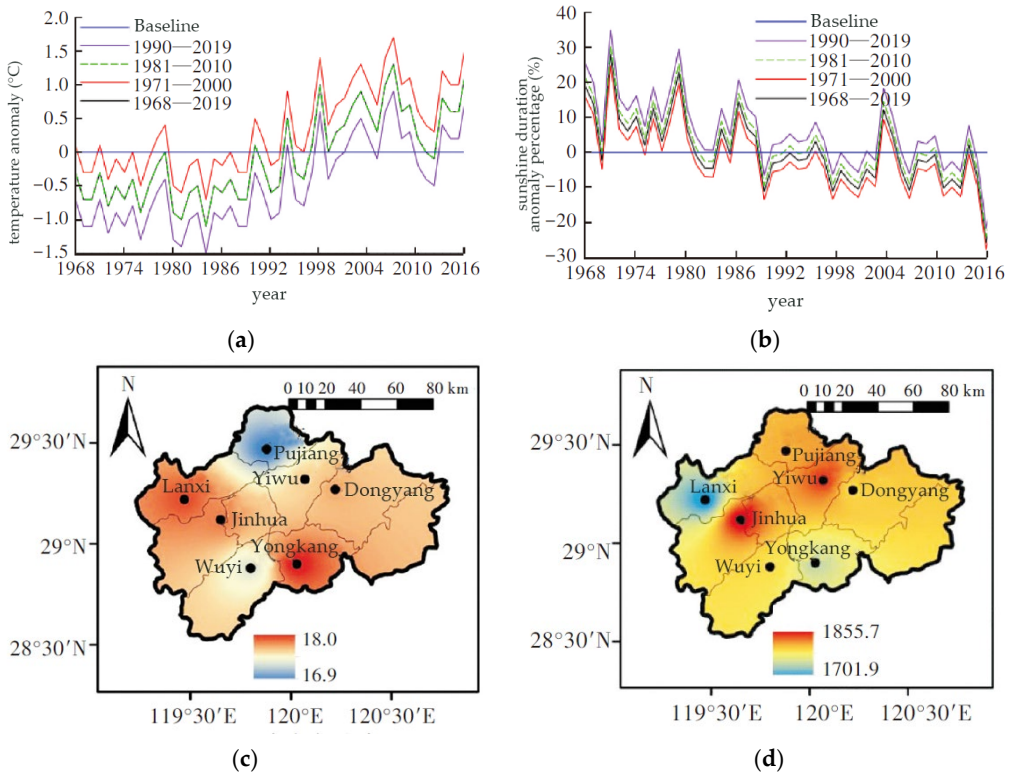


Figure 1. Interannual variations of temperature and sunshine duration in Jinhua under different climate normals. (**a**) Interannual variations of temperature anomaly; (**b**) interannual variations of sunshine duration anomaly percentage; (**c**) spatial variation of temperature in Jinhua under the climatic normal; (**d**) spatial variation of sunshine duration in Jinhua under the climatic normal.

2.2. Typological Study and Case Selection

2.2.1. Prototype

The Thirteen-Bay House is traditionally recognized as a two-story complex, comprising a main hall and two lateral chambers, each consisting of three bays. These lateral chambers are connected to the main hall via "dongtouwu" (flanking room), with all elements linked through transitional eave galleries (Figure 2a). The central bay of the main hall generally functions as an open area without partition walls. Extending along the axial direction, the structure further develops into the Eighteen-Bay House or Twenty-Four-Bay

House. The former can be regarded as a combination of one complete prototype and a half prototype, while the latter comprises two prototype units connected in series (Figure 2b). A small skywell may be inserted between the gable wall of the main hall and the connecting galleries; additionally, between serially connected units, supplementary galleries or second-story passageways may be incorporated (Figure 2c).

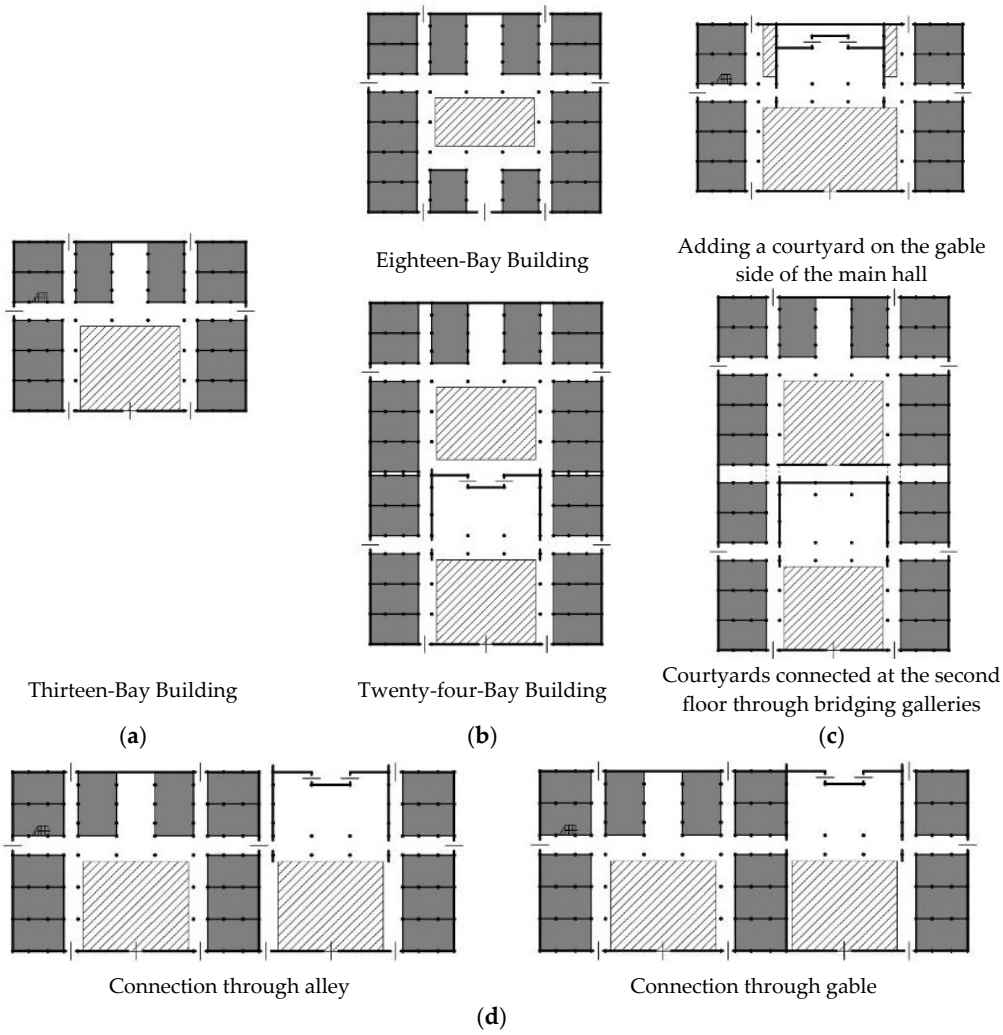


Figure 2. (**a**) Prototype unit; (**b**) longitudinal expansion of units; (**c**) variants of the unit; (**d**) lateral assembly of units.

When assembled laterally, one prototype unit functions as the main body, while a second unit removes one side chamber prior to attachment to the first. The gable wall of the second main hall may either leave an alley between it and the adjacent chamber or connect directly to it (Figure 2d).

The spatial prototype of the Thirteen-Bay House was derived by concentrating on architectural elements related to transitional space—such as columns, walls, fully enclosed "rooms" with complete climatic boundaries, open-air courtyards, and covered yet semi-open areas including eaves galleries and halls. Shaded areas represent fully enclosedrooms with climatic boundaries; diagonally hatched areas denote courtyards; unshaded areas indicate eaves galleries or halls.

2.2.2. Case Selection of Representative Example

The Lu Residence (Luzhai), situated in Dongyang, Zhejiang Province, under the jurisdiction of Jinhua, stands as the largest and most well-preserved Ming–Qing period

residential complex within the Jiangnan region. Geographically, it is characterized as facing Bijiashan Mountain to the south, with the Dongyang River to the north, and flanked by the Yaxi stream on both sides, all set within a scenic landscape. The Lu clan established their settlement in this location during the Song dynasty and experienced prosperity throughout the Ming and Qing dynasties. Influenced by clan-based settlement patterns and patriarchal customs, the complex was constructed with the Suyongtang Hall serving as its central structure, with spatial arrangements reflecting lineage hierarchy and official rank. Multiple subsidiary axes extended to the east and west of the core area.

The Suyongtang Hall axis predominantly functioned as a residential and ceremonial zone for large-scale activities (Figure 3a). The eastern and western sectors were chiefly residential and adhered to the traditional arrangement of "ancestral hall on the left, temples on the right": the east side was home to the Grand Ancestral Hall of the Lu Clan in Yaxi, whereas the western side accommodated various temples, including the Bronze Buddha Hall and the Guandi Temple. The southern plots were designated for agricultural cultivation, while the northern plots were reserved for farmland and gardens. Consequently, the entire compound integrated residential, recreational, educational, ancestral, and religious functions, thereby comprehensively supporting the needs of clan-based communal living.



(**a**) (**b**) (**c**)

Figure 3. (**a**) Original plan; (**b**) present aerial photograph; (**c**) present condition photos.

This study concentrates on the residential area situated behind the stone gate of the Suyongtang Hall axis. Currently, this section is relatively well preserved (Figure 3b), though the central hall located behind the stone gate has collapsed. Presently, the Lu Residence primarily serves as a tourist exhibition space: its interiors remain incomplete, lacking suspended ceilings or decorative finishes, and are furnished with minimal furniture. The ground-floor windows and doors are kept open, while the second floor remains inaccessible to visitors (Figure 3c). Considering its typological characteristics, scale, and condition, the Lu Residence has been selected as a representative case for field investigation in this study.

2.3. Research Framework

This study concentrates on the transitional space within traditional courtyard dwellings at the Lu Residence in Dongyang, Jinhua, with particular emphasis on their climatic adaptability in regions characterized by hot summers and cold winters. Utilizing typological analysis, principles of passive green design, field measurements, computer simulation and optimization, and comparative analysis, the research seeks to elucidate

the coupling mechanisms between the architectural form of transitional space and the multi-physical fields of wind, light, and heat.

2.3.1. Evaluation Standards for Transitional Space Environments

Existing evaluation systems for the built environment are not fully applicable to traditional dwellings and the transitional space that forms the focus of this study. Therefore, this research integrates the Assessment Standard for Green Buildings (GB/T 50378-2019) [36] and the thermal comfort indices PMV–PPD as reference indicators.

According to GB/T 50378-2019, outdoor wind environment evaluation is defined as follows:

- Winter conditions (typical wind speed and direction):
    1. Pedestrian areas around buildings should have wind speeds lower than 5 m/s, and the outdoor wind amplification factor should be less than 2.
    2. Except for the first row of windward buildings, the pressure difference between windward and leeward building surfaces should not exceed 5 Pa.
- Transitional and summer conditions (typical wind speed and direction):
    3. No vortices or stagnant wind zones should appear in pedestrian activity areas within the site.
    4. More than 50% of openable windows should have a pressure difference greater than 0.5 Pa on their interior surfaces.

In indoor environments, when air velocity falls below 0.25 m/s, human occupants generally cannot perceive airflow. When it ranges between 0.25 m/s and 0.5 m/s, it is commonly perceived as comfortable, with daily activities and emotions remaining unaffected. Based on this criterion, wind velocity zones are classified into three categories: still-air zone (velocity < 0.25 m/s), comfort zone (0.25–0.5 m/s), and strong-wind zone (velocity > 0.5 m/s). The proportion of each zone is calculated, with a higher percentage of the comfort zone indicating a more favorable wind environment.

Thermal comfort is influenced by air temperature, mean radiant temperature, relative humidity, airflow velocity, metabolic rate, and clothing insulation, with the first four being environmental physical variables. Research shows that optimal indoor temperatures are around 25 °C, while discomfort arises below 12 °C or above 30 °C. Within a relative humidity of 40–70%, evaporation remains stable; however, at higher humidity, lower wind speeds impede evaporative heat dissipation, reducing comfort. When relative humidity exceeds 70%, discomfort increases significantly with rising humidity levels.

Owing to material limitations and the lack of contemporary heating and cooling systems, traditional residences demonstrate a restricted ability to control the climate. Consequently, indoor temperature and humidity during extreme months seldom satisfy current comfort standards. This study, therefore, emphasizes daytime variations of key indicators by comparing data from various measurement points within the same timeframe and applying pertinent standards to assess the collected data.

2.3.2. Quantification of Research Subjects Through Field Measurements

The field investigation was composed of two primary components:

1. Surveying and mapping the complex plans (Figure 4a), compiling fundamental information about the buildings (Table 1) and courtyards (Table 2), and subsequently constructing three-dimensional models utilizing Rhinoceros (Figure 4b).
2. Deployment of measurement points and the collection of environmental data were conducted. The measurement points were distributed as illustrated in Figure 4c and classified into four distinct categories.

a Type I: Temperature–humidity loggers were deployed at the beginning of the survey to record diurnal variations automatically.
b Type II: Thermal comfort recorders are systematically placed at each location for a duration of 5 min to automatically record temperature, humidity, and air velocity. Furthermore, solar radiation was measured manually at points A, B, and C.
c Type III: Manual measurement of solar radiation.
d Type IV: Manual measurement of indoor and outdoor wall surface temperatures.

Climatic conditions during the survey were as follows:

- On 26 December, the weather was characterized by overcast skies with light rain during the afternoon. Temperatures ranged from 3 to 12 °C. Westerly winds were observed at Beaufort scale levels 4 to 5.
- On 27 December, the sky was clear, with temperatures ranging from 2 to 9 °C. There was no prevailing wind, and the wind speed was recorded on the Beaufort scale as 1 to 2.

The geographical coordinates of the Lu Residence are 120°15′13.29″ E, 29°16′6.08″ N. Based on this location, the solar altitude angle during the survey was calculated at 37.35°, with a day length of 9.6 h.

The instruments used in the field investigation are listed in Table 3.

Table 1. Basic information about buildings.

Building	Bay	Stories	Width	Depth	1F Height	W/D Ratio	H/D Ratio	Roof Type	Roof Pitch
Leshoutang Hall	5	2	20,300	7000	2750	2.9	0.39	Overhanging Gable	25°
Gatehouse	3	1	11,890	6350	3200	1.87	0.5	Flush Gable	26°
Shiyongtang Hall	3	1	11,890	7690	6720	1.55	0.87	Flush Gable	28°
Side Chamber of Leshoutang Hall	2	1	5000	3790	4240	1.32	1.09	Overhanging Gable	20°
Side Chamber	5	2	2900~3870	5540	3000	0.52~0.7	0.54	Flush Gable	27°

Table 2. Basic information about courtyards.

		A	B	C
Width		11,980	12,340	12,340
Depth		5550	7600	8200
W/D Ratio		2.16	1.62	1.5
2F Eave Height (South)/Depth		0.9	0.68	0.63
Eave Height/Overhang Width (H/W Ratio)	North	4500/2360 = 1.91	3810/1040 = 3.66	4480/1050 = 4.27
	South	3920/1100 = 3.56	3360/1040 = 3.23	3500/700 = 5
	West	3760/760 = 4.95	3520/950 = 3.71	3510/1950 = 1.8
	East	3760/760 = 4.95	3520/1040 = 3.38	3510/1970 = 1.78

Table 3. Instruments used in the field investigation.

Instrument	Image	Accuracy	Measuring Range	Application
SSDZY-1 Thermal Comfort Recorder (Beijing Tianjian Huayi Technology Development Co., Ltd., Beijing, China)		Temperature: ±0.3 °C Relative Humidity: ±2% (10–90% RH) Globe Temperature: ±0.3 °C Air Velocity: 5% ± 0.05 m/s	Temperature range: –20 °C to 80 °C Relative Humidity range: 0.01% to 99.9% RH Globe Temperature range: –20 °C to 80 °C Air Velocity range: 0.05 m/s to 5 m/s	Automatic recording of temperature, relative humidity, and air velocity

Table 3. *Cont.*

Instrument	Image	Accuracy	Measuring Range	Application
Elitech GSP-6 Temperature–Humidity Logger (Elitech Technology Co., Ltd., Jiangsu, China)		Temperature: ±0.5 °C Relative Humidity: ±3% RH	Temperature range: −35 °C to 80 °C Relative Humidity range: 0% to 100% RH	Automatic recording of temperature and relative humidity
TES-132 Solar Power Meter (TES Electronic Industrial Co., Ltd., Taipei, Taiwan)		±10 W/m^2 or ±5% (the larger value applies)	0~2000 W/m^2	Manual measurement of solar radiation
Fluke 561 Infrared Thermometer (Fluke Corporation, Everett, WA, USA)		±1% or ±1 °C (the larger value applies)	−40~+550 °C	Manual measurement of surface temperature
Leica D510 Laser Distance Meter (Leica Geosystems, Heerbrugg, Switzerland)		±1.0 mm	0.05~200 m	Manual measurement of distance

By analyzing the surveyed architectural information in conjunction with the collected environmental data, correlations were identified to derive qualitative conclusions and establish the scope for subsequent quantitative analysis.

2.3.3. Comparative Simulation Analysis for Establishing Climatic Adaptation Prototype

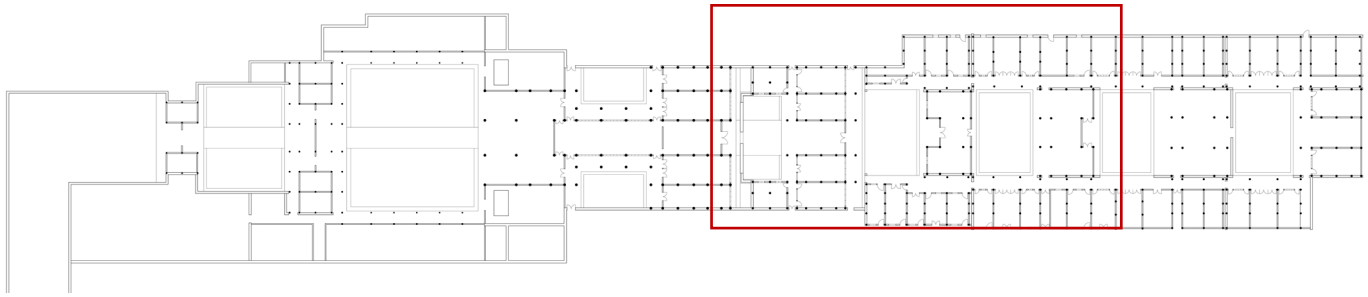
1 CFD Simulation

This study utilized the PHOENICS 2016 to simulate the wind environment of the case study. The parameters were configured in accordance with the Beijing Green Building Design Standard (DB11) [37].

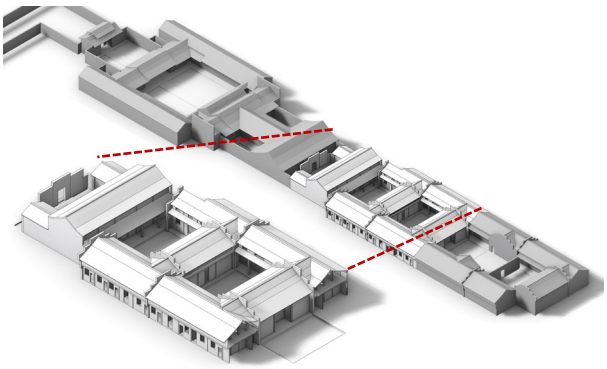
- Computational Domain: The length and width were set to five times the model size, and the height to four times the building height (4H).
- Grid Division: PASOL was used to optimize grid quality. Three schemes were tested, with the grid numbers in each direction following a 1.5 ratio. Grid independence was verified before finalizing the division.
- Boundary Conditions: Wind speed was established based on the annual average data provided by the local meteorological station. A power-law profile was employed, with the exponent and surface roughness tailored to the specific circumstances. Symmetry boundary conditions were applied to the upper and lateral boundaries.
- Convergence Criteria: Simulations were deemed converged when oscillations were minimal and the root-mean-square residuals dropped below 0.001.
- Turbulence Model: The k–ε model was selected since the studied dwellings are low-rise (1–2 stories), and the focus is on ground-level wind variation.
- Discretization Scheme: The QUICK format was adopted.

2. Solar Radiation Simulation

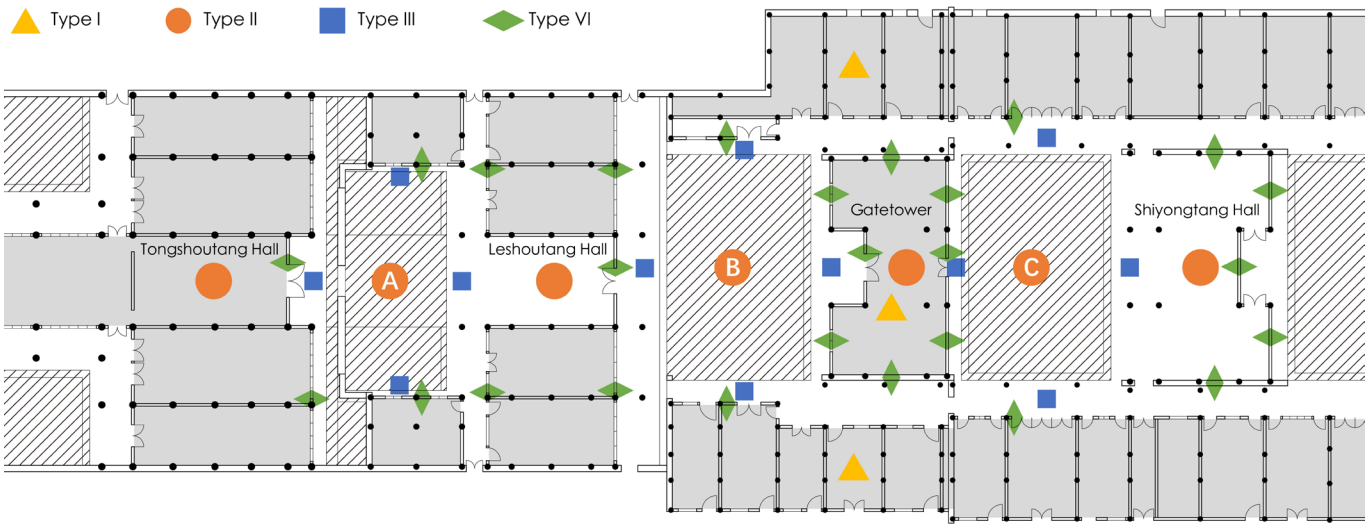
Solar radiation simulations were conducted utilizing Revit Insight360, based on meteorological data concerning local solar radiation. These simulations calculated the theoretical solar heat gain of the study objects under various conditions.



(**a**)



(**b**)



(**c**)

Figure 4. (**a**) Measured floor plan with the red box indicating the area where the environmental measurements were conducted; (**b**) three-dimensional model and enlarged view of the measured area; (**c**) layout of measurement points. Gray-filled areas represent indoor spaces, hatched areas indicate courtyards, and white areas denote transitional spaces. The letters within the orange circles indicate the courtyard labels.

2.3.4. Practical Application of the Climatic Adaptation Prototype

The climatic adaptation prototype derived from simulation serves as prescriptive guidelines that can inform the determination of environmentally optimal forms in real projects. One practical application is a new guesthouse project adjacent to a protected heritage site in the Liberation Street Historic District of Yongkang, Jinhua. Due to the requirements of preserving historical context, the project was obliged to adopt the traditional dwelling morphology. The findings of the present study were applied in the early stage of

master planning, providing spatial control measures that ensure a favorable baseline for environmental comfort once the building is occupied. Thus, the proposed mechanism of "regional climate–transitional space morphology" matching provides a practical pathway for the scientific continuation of the Thirteen-Bay House as a representative type of Jinhua's traditional dwellings.

3. Field Investigation and Measurements

3.1. Wind Environment

Figure 5 shows that throughout all measurement points, wind speed remained consistently below 0.6 m/s. Specifically, in Tongshoutang Hall and Shiyongtang Hall, wind speeds were predominantly under 0.25 m/s, indicating minimal air circulation. At the remaining locations, average wind speeds for the majority of the observed period were within the comfort threshold.

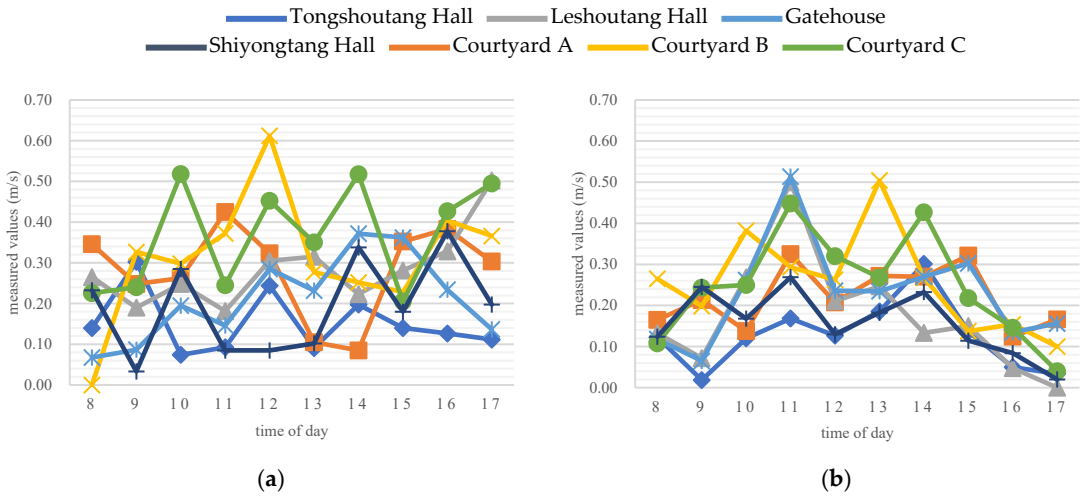


Figure 5. Measured wind speed. (**a**) Wind speed variation curve on December 26; (**b**) Wind speed variation curve on December 27.

3.2. Light Environment

Figure 6 shows that, under overcast conditions, solar radiation at courtyard measurement points consistently remains below 75 W/m^2, whereas it remains below 25 W/m^2 beneath the eaves, demonstrating minimal variation across various orientations.

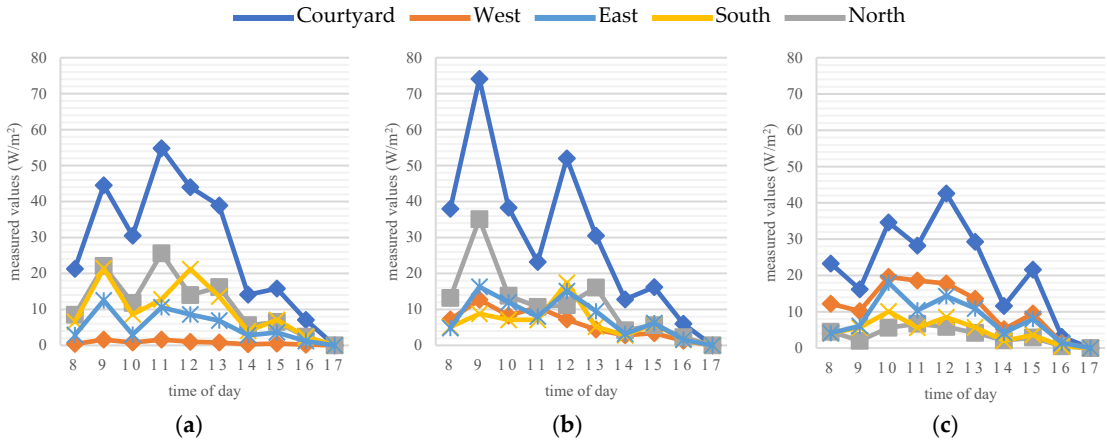


Figure 6. Measured solar radiation on December 26. (**a**) Solar radiation variation curve of Courtyard A; (**b**) solar radiation variation curve of Courtyard B; (**c**) solar radiation variation curve of Courtyard C.

Figure 7 shows that, under sunny conditions, solar radiation at courtyard measurement points ranges from 320 to 520 W/m^2 when exposed to direct sunlight. Conversely, when shaded, the radiation fluctuates between 5 and 45 W/m^2. Before 9:00–11:00, the radiation intensity follows the sequence within the same courtyard: west eave > north eave > east eave > south eave. Subsequently, the sequence shifts to: north eave > west eave > east eave > south eave. The solar radiation beneath the east and south eaves exhibits only minor fluctuations, with the east eave receiving nearly three times the radiation compared to the south eave. At the west eave, the radiation levels prior to 9:00–11:00 are comparable to those at the courtyard center, but thereafter, they decrease to levels akin to those under the east and south eaves. The north eave maintains relatively high radiation levels from 9:00 to 14:00.

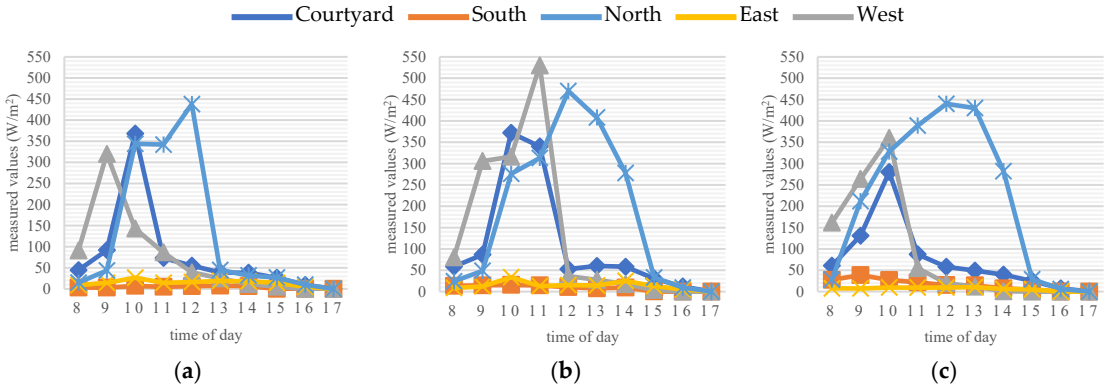


Figure 7. Measured solar radiation on December 27. (**a**) Solar radiation variation curve of Courtyard A; (**b**) solar radiation variation curve of Courtyard B; (**c**) solar radiation variation curve of Courtyard C.

3.3. Thermal Environment

3.3.1. Temperature–Humidity in Courtyard and Building

The measurements of daytime temperature and humidity within the courtyards were utilized to analyze thermal environmental variations. Figure 8 shows that during overcast or rainy days, differences among courtyards were minimal, with stable daytime fluctuations. Temperature variations remained within 3 °C, and humidity levels ranged from 86% to 91% relative humidity. Conversely, on sunny days, courtyard temperatures exhibited more substantial fluctuations, with daytime differences of 4–7 °C. A notable increase was observed around 10:00–11:00 a.m., corresponding to measured solar radiation. Peak temperatures were recorded between 2:00–3:00 p.m., whereas humidity differences reached approximately 20% relative humidity.

Measurements of daytime temperature–humidity in axis-aligned halls were analyzed to compare the thermal environments of halls at different locations within the complex. Figure 9 shows that on overcast days, indoor values closely corresponded with those of the adjacent southern courtyards. On sunny days, indoor temperatures increased from 8:00 a.m. to 3:00 p.m. and subsequently declined, with daytime temperature differences of 5–7 °C and humidity variations of approximately 20% RH. Prior to 9:00 a.m. and following 4:00 p.m., inter-building variations were minimal; however, fluctuations between 9:00 a.m. and 4:00 p.m. were significant. The comparisons indicate that indoor temperatures exhibited a positive correlation with solar radiation received by the north eave.

A comparison was conducted among three buildings situated on the south, west, and east sides of Courtyard B, analyzing their indoor temperature and humidity variations over the period of 27 December. Figure 10 shows that for the side chambers and the main hall of a courtyard group, the morning temperature sequence is: eastern chamber > western chamber > main hall; in the afternoon: main hall > eastern chamber > western chamber;

and in the evening: western chamber > Gatehouse > eastern chamber. The daytime temperature difference of the side chambers remains within 6 °C, whereas that of the main hall reaches 15 °C, with a maximum of nearly 22 °C at 14:00. The indoor temperature of the buildings exceeds the outdoor temperature by more than 1 °C, while humidity differences are insignificant.

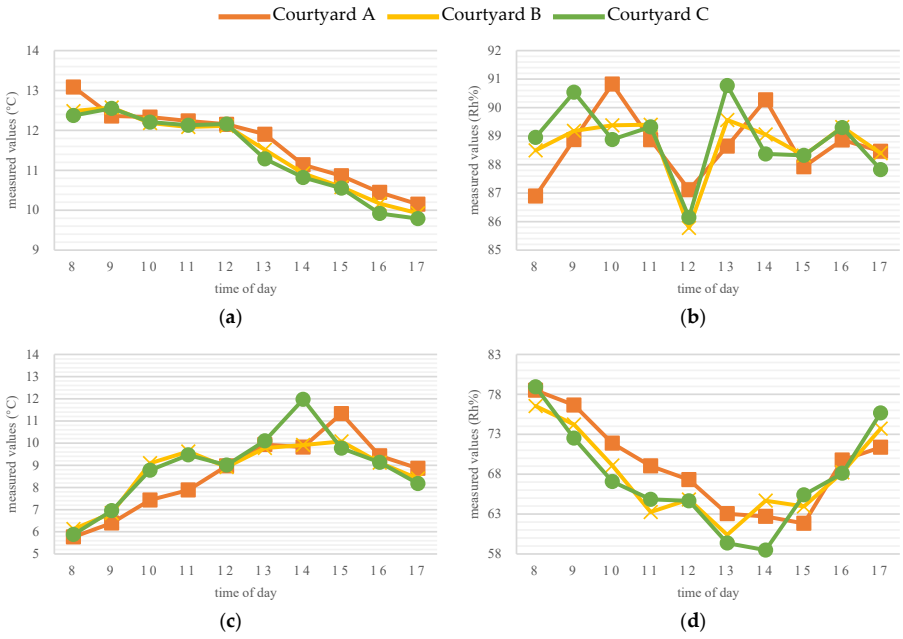


Figure 8. Measured temperatures and humidity in courtyards. (**a**) Temperature variation curve on 26 December; (**b**) humidity variation curve on 26 December; (**c**) temperature variation curve on 27 December; (**d**) humidity variation curve on 27 December.

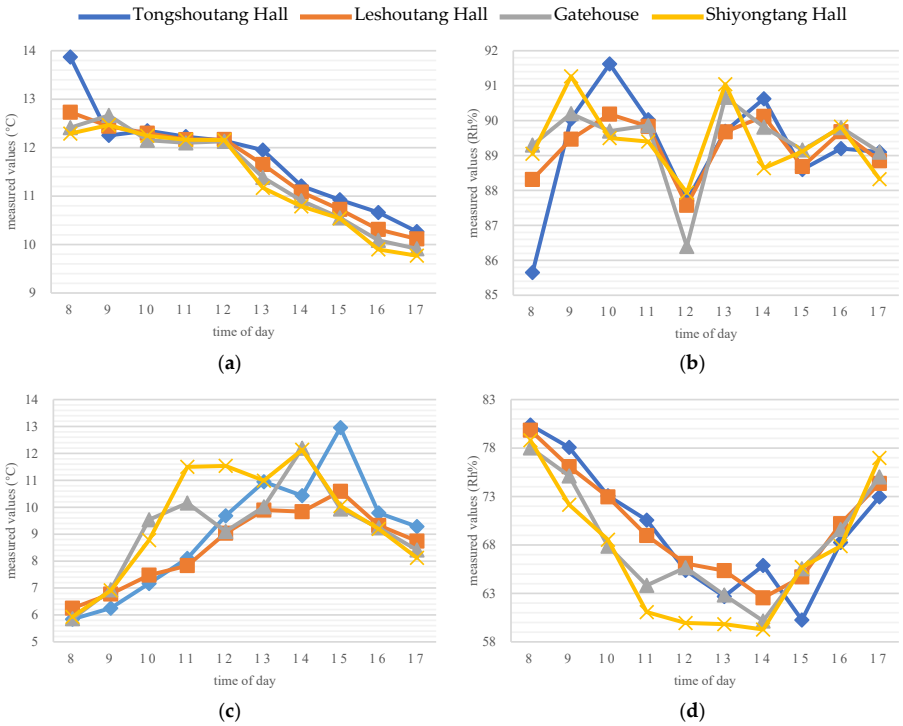
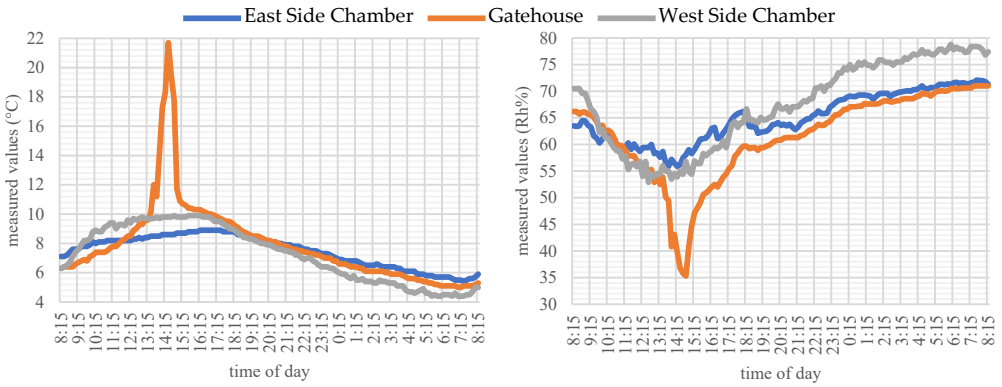


Figure 9. Measured temperatures and humidity in halls. (**a**) Temperature variation curve on 26 December; (**b**) humidity variation curve on 26 December; (**c**) temperature variation curve on 27 December; (**d**) humidity variation curve on 27 December.



(**a**) (**b**)

Figure 10. Measured temperatures and humidity in three buildings of Courtyard B. (**a**) Temperature variation curve during 26–27 December; (**b**) humidity variation curve during 26–27 December.

3.3.2. Heat Gains of Building Interfaces

The survey revealed that on the 26th, under overcast conditions accompanied by light rain, the wall-surface temperatures across all measurement points remained consistent at approximately 13 °C in the morning and around 11 °C in the afternoon, exhibiting negligible variation among different locations and materials. Conversely, on the 27th, under clear, sunny conditions, the measured temperatures experienced substantial fluctuations, as detailed below.

(1) Courtyard Interfaces

The principal façades of the Lu Residence's main courtyard are primarily constructed of timber, timber with a white plaster finish, and grey brick. At the midpoint of each façade—typically aligned with wooden door panels—surface temperatures were recorded to assess solar heat gain (Figure 11). Before 09:00–12:00, the wall-surface temperatures in the courtyards follow the sequence: west > north > east > south; subsequently, this sequence shifts to: north > west > east > south. The peak temperature of the west façade is recorded at 09:00, whereas that of the north façade occurs at 14:00, with the northern surface exhibiting higher temperatures than the western. The variations in maximum temperatures are influenced by courtyard dimensions and the depth of eave overhangs. During the daytime, the temperature fluctuations of the south and east façades remain within 5 °C, showing minimal differences across the courtyards. The pattern of wall-surface temperature variation for each façade correlates with the solar radiation received beneath the eaves.

(2) Axial Building Interfaces

Among the axial buildings within the survey scope, only Gatehouse possesses a complete climatic boundary and exhibits relative independence; consequently, it was selected as the research subject. The central sections of its south and north façades are constructed of timber, whereas the east and west façades are built of grey bricks. Field measurements of the interior and exterior wall-surface temperatures at the midpoints of each of the four façades of Gatehouse were conducted to analyze the heat gain of each façade.

Figure 12 shows that the exterior wall-surface temperatures of Gatehouse follow the hierarchy: west > east, and south > north. The brick walls on the east and west sides remain relatively stable throughout the day at 8–9.5 °C. On the north side, the daytime temperature difference reaches 4 °C, with a peak of 9 °C at 14:00. On the south side, the temperature increases sharply between 11:00 and 14:00, attaining a maximum of 34.5 °C at 14:00, resulting in a daytime differential of 27 °C. Regarding the interior wall surfaces,

before 12:00, the temperature order is east ≈ west > south ≈ north; after 12:00, it shifts to south > north > west > east. The exterior wall temperature on the south side exceeds the interior temperature before 12:00, with a maximum difference of 20 °C; at 14:00, both interior and exterior temperatures reach their peaks, with an 8 °C differential. For the remaining façades, interior wall temperatures consistently remain higher than exterior temperatures. These findings suggest that the main hall along the axis predominantly receives solar radiation through the south façade. After 12:00, as indoor temperatures increase, the interior wall temperatures of all façades also rise accordingly.

The secondary bays of Gatehouse's southern façade are composed of various materials: grey brick beneath the windowsills, white-plastered timber above, and timber window frames. Figure 13 shows that, for the same façade, timber with a white plaster finish exhibits the lowest temperature. At 12:00 (the western chamber) and prior to 15:00 (the eastern chamber), the wall-surface temperature of raw timber is higher than that of grey brick; subsequently, the temperature of the grey brick surpasses that of raw timber. Among the maximum temperatures recorded for different materials, raw timber exceeds grey brick, which in turn exceeds timber with a white plaster finish. Raw timber heats rapidly but possesses poor thermal inertia, whereas grey brick demonstrates notable thermal inertia. The plaster finish can enhance the thermal inertia of timber, although it significantly diminishes its heat-gain capacity.

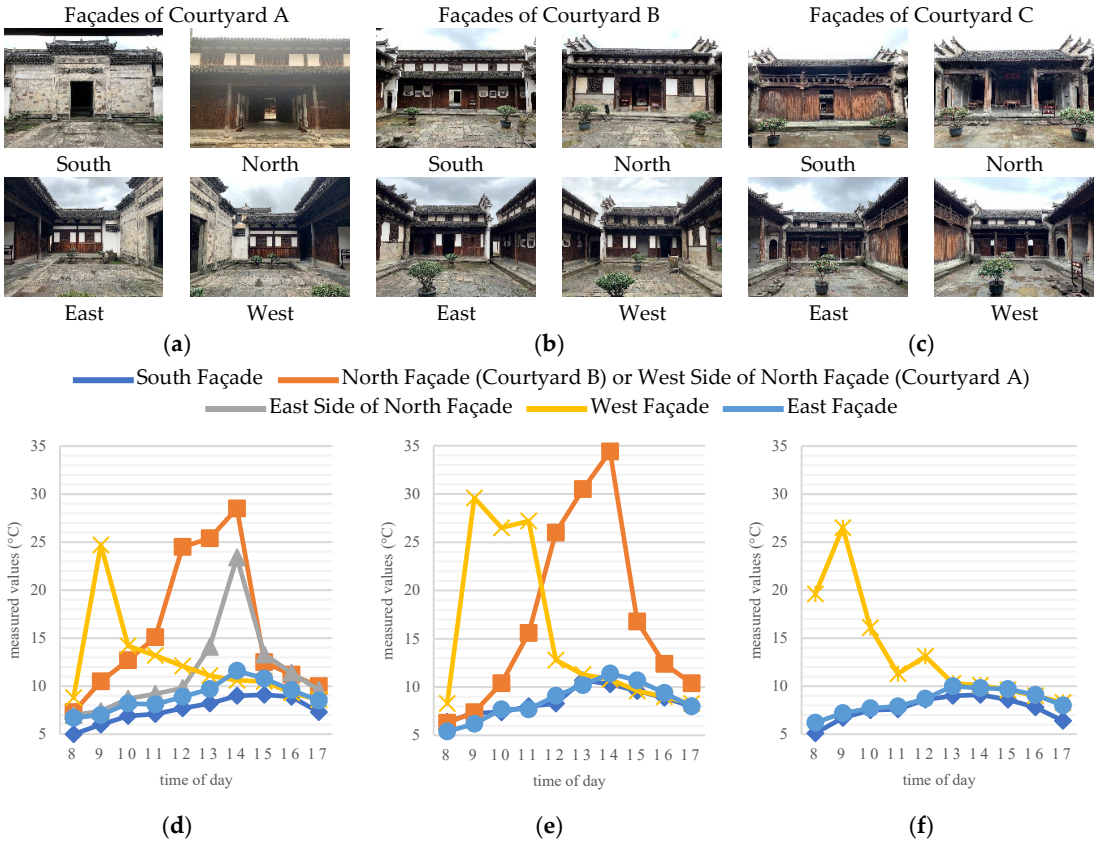


Figure 11. Measured wall-surface temperatures in courtyards. (**a**) Façades of Courtyard A; (**b**) façades of Courtyard B; (**c**) façades of Courtyard C; (**d**) wall-surface temperature variation curve of Courtyard A; (**e**) wall-surface temperature variation curve of Courtyard B; (**f**) wall-surface temperature variation curve of Courtyard C.

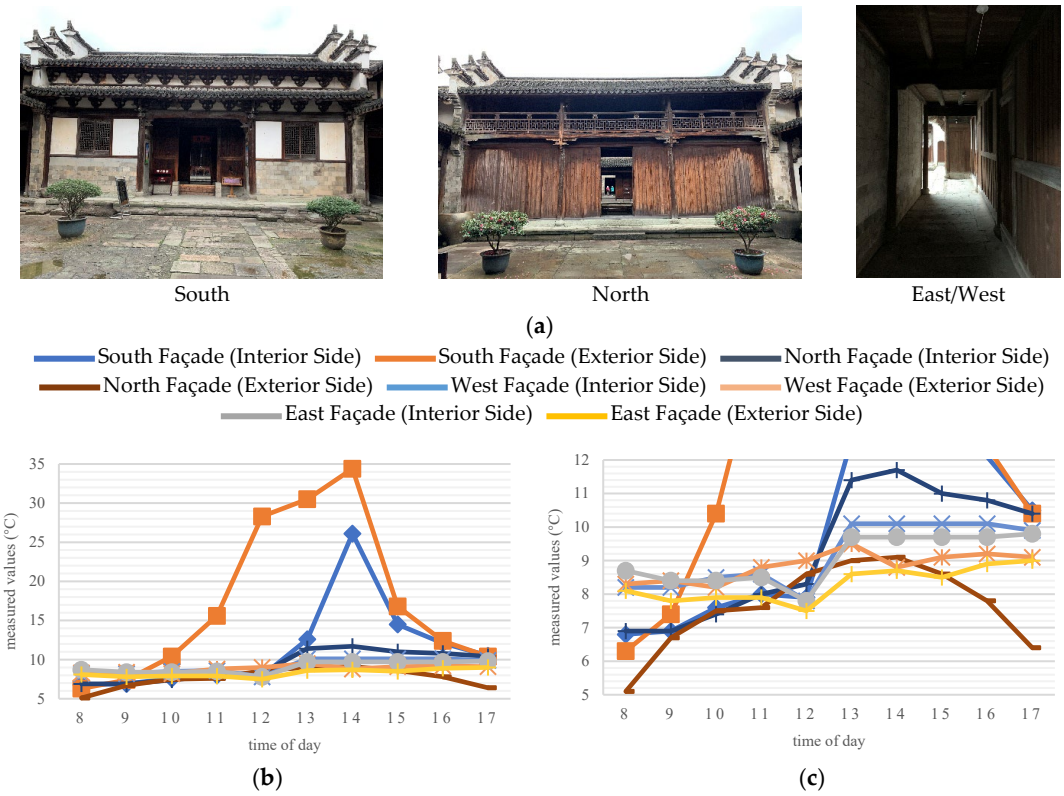


Figure 12. Measured wall-surface temperatures of Gatehouse. (**a**) Façades of Gatehouse; (**b**) wall-surface temperature variation curve of Gatehouse; (**c**) enlarged view of the curve.

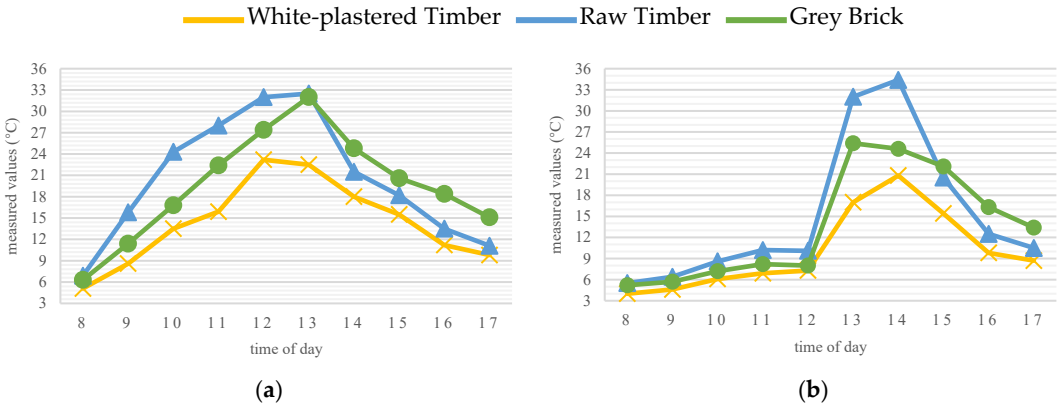


Figure 13. Measured wall-surface temperatures of Gatehouse's southern façade. (**a**) Wall-surface temperature variation curve of the western chamber of Gatehouse; (**b**) wall-surface temperature variation curve of the eastern chamber of Gatehouse.

(3) Chamber Interfaces

The façades of both the eastern and western chambers are entirely fabricated from timber. Field measurements were carried out on the interior and exterior façades of the eastern and western chambers of the Gatehouse, in addition to Courtyards B and C, to evaluate the impact of direct solar radiation on façade heat gain and heat transfer.

Figure 14 shows that the side chambers situated on both sides of the building do not receive direct solar radiation throughout the day, resulting in only minor fluctuations in wall-surface temperatures. For the side chambers adjacent to the courtyard, the wall-surface temperature of the western chamber exceeds that of the eastern chamber. The temperature in the western chamber peaks between 09:00 and 11:00, followed by a sharp decline, with a

daytime temperature difference of approximately 20 °C. Conversely, the eastern chamber exhibits a gradual increase in temperature throughout the day, reaching its peak at 14:00, with a temperature difference of roughly 5 °C. The observed variation in wall-surface temperature aligns with the pattern of solar radiation beneath the eaves. Furthermore, although Courtyards B and C possess identical widths, the eave-gallery height-to-width ratio of the side chambers in Courtyard B is twice that of Courtyard C, contributing to differences in heat gain. When subjected to direct solar radiation, the exterior wall-surface temperature can reach up to 10 °C higher than the interior surface; however, at other times, the interior wall-surface temperature generally surpasses that of the exterior.

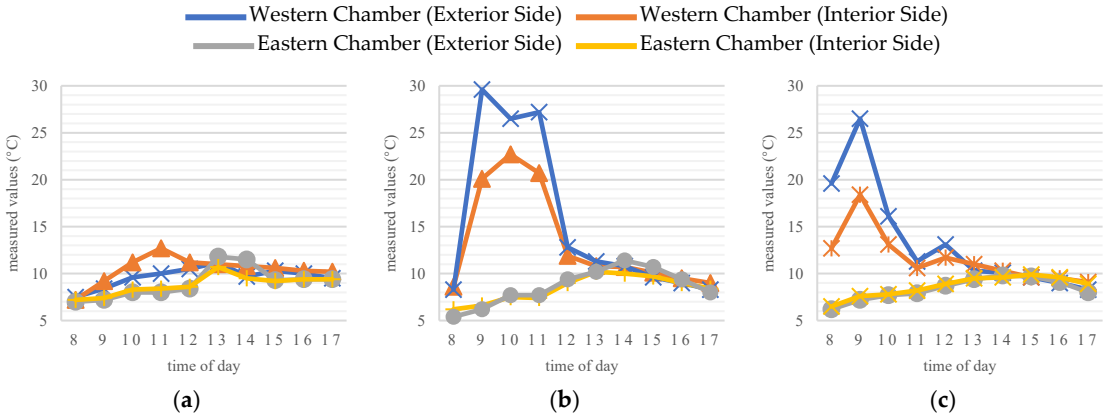


Figure 14. Measured wall-surface temperatures of chambers flanking Gatehouse. (**a**) Wall-surface temperature variation curve of the chambers flanking Gatehouse; (**b**) wall-surface temperature variation curve of the chambers flanking Courtyard B; (**c**) wall-surface temperature variation curve of the chambers flanking Courtyard C.

3.4. Comprehensive Analysis

Through architectural surveying and environmental measurements, morphological parameters were paired with environmental parameters for comparative analysis. Preliminary findings reveal correlations between geometric form and climatic adaptability.

1. Ensemble

In courtyards within the cluster, solar radiation on facades and rooftops constitutes the primary source of heat gain. Given that each building generally has approximately half of its roof directly exposed to sunlight, roof heat gain can be regarded as roughly equivalent throughout the cluster. Consequently, exposure of the facades predominantly influences variations in thermal performance. The Lu Residence is oriented approximately 30° west of due south, which enhances solar gain on the chambers and accentuates the differences between the eastern and western chambers. Since this deviation is less than 45°, south-facing facades continue to receive more solar radiation than east-facing ones.

A building's placement within the cluster affects its thermal stability: centrally located structures demonstrate greater thermal stability than those situated at the periphery. Furthermore, a higher proportion of courtyard-facing facades, relative to the total envelope area, correlates with decreased thermal stability. During the winter season, internal hall temperatures are relatively elevated during daytime, while the chambers within clusters tend to cool more slowly at night, thereby maintaining higher nighttime temperatures compared to halls. This observation aligns with spatial usage patterns, wherein the chambers function as sleeping quarters during the night and the halls serve as living spaces during daylight hours.

2. Courtyard

When subjected to direct sunlight, indoor temperatures surpass outdoor temperatures, owing to less efficient convective heat dissipation within indoor environments and increased heat accumulation. The narrow, elongated courtyards within residential zones facilitate greater north–south separation, thereby augmenting solar heat gain for both the courtyards and interior spaces during the winter season.

Courtyard proportions influence both indoor and outdoor temperatures: hall temperature is inversely correlated with the height-to-width ratio of the southern courtyard, and courtyard temperature is inversely correlated with the courtyard height-to-width ratio. Thus, courtyard dimensions directly affect solar heat gain on building interfaces.

3. Eave Gallery

Beginning from the second courtyard behind the stone gate, uninterrupted single-story eave galleries are flanked by two-story chambers. These chambers serve as windbreaks, leading to reduced wind speeds within the courtyards situated further inward of the cluster. Concurrently, the continuous galleries function as wind channels, where airflow velocities are three to five times greater than those observed within the courtyards. On the western and northern sides of the courtyards, the eave galleries additionally provide shading, thereby significantly affecting façade heat gain.

The preliminary field investigation demonstrates the role of building form as a climatic regulator during the winter season. These findings identify key variables for simulation—including orientation, courtyard proportions, and eave depth—and emphasize the study's spatial and temporal limitations, specifically that measurements were limited to a single season (winter) and local sampling points. Consequently, subsequent computer simulations were conducted to develop multi-scenario comparisons, verify correlations, and optimize parameters for climatic adaptability.

4. Simulation and Optimization

Owing to the interactions among wind, light, and thermal environments, when an architectural element influences one environmental parameter, it consequently affects another indirectly. For example, the duration of solar exposure impacts solar radiation heat gain, which is directly associated with temperature; temperature discrepancies influence stack ventilation, which has a direct relationship with airflow; and solar exposure indirectly affects ventilation by modifying temperature. Therefore, a single architectural element may impact multiple environmental factors through these interconnected mechanisms. Based on the survey findings discussed above, the correlations between building and environmental factors are summarized in Table 4, where "●" signifies direct influence, "○" signifies indirect influence, and "-" indicates a relatively weak correlation.

Table 4. Correlation between architectural elements and environmental factors.

Architectural Elements		Outdoor Environment			Indoor Environment		
		Light	Thermal	Wind	Light	Thermal	Wind
Ensemble	Orientation	●	○	●	●	○	○
Courtyard	Layout	●	○	●	●	○	-
	Proportion	●	○	●	●	○	-
Eave Gallery	Layout	-	-	●	-	-	-
	Proportion	●	○	-	●	○	-

4.1. Ensemble

4.1.1. Orientation and Wind Environment

(1) Correlation between Prototype Model and Case Model

The Shiyongtang courtyard of the Lu Residence was selected as a representative case for analysis. Wind environment simulations were performed under identical boundary conditions to those employed for the prototype model. Ten measurement points were designated to record the simulated wind velocities, which were subsequently analyzed through correlation analysis. As illustrated in Figure 15, the R^2 value is 0.86, denoting that the similarity between the simulated results of the actual model and the prototype model is 86.0%. The significance F value is 0.0008 (Table 5), confirming the overall significance of the regression model.

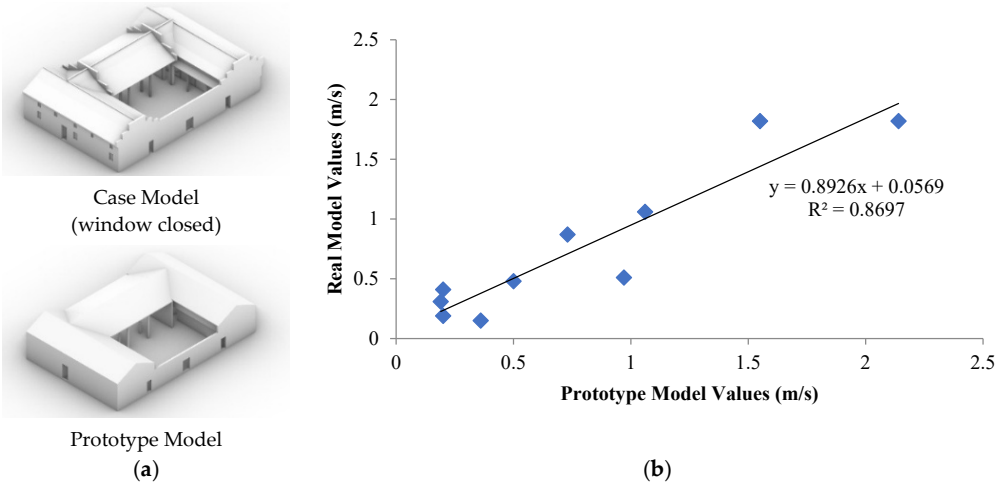


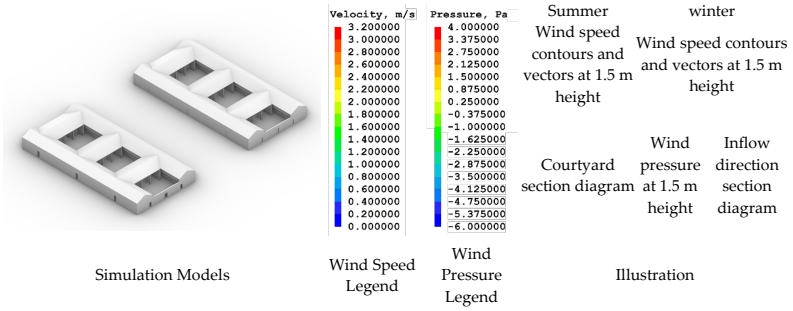
Figure 15. (**a**) Models used for stimulation; (**b**) linear regression plot of case model and prototype model wind values.

Table 5. ANOVA.

	df	Sum of Squares	Mean Squared	F	Significance F
Regression	1	3.05	3.05	53.41	0.0008
Residual	8	0.46	0.06		
Total	9	3.51			

(2) Prototype Model Simulation

Buildings located in regions characterized by hot summers and cold winters must sufficiently balance wind protection during winter with ventilation necessities in the summer season. The average annual wind speed in Jinhua is documented at 2.7 m/s. Employing the conventional growth model of the prototype, which consists of three sequentially connected courtyards, simulations were performed with varying angles between the prevailing wind direction and the building orientation, ranging from 0° to 180°. For summer conditions, the main gate was modeled as open; in contrast, during winter, it was modeled as closed. The input wind speed was standardized at 2.7 m/s. The results of the simulations are presented in Figure 16.



(**a**)

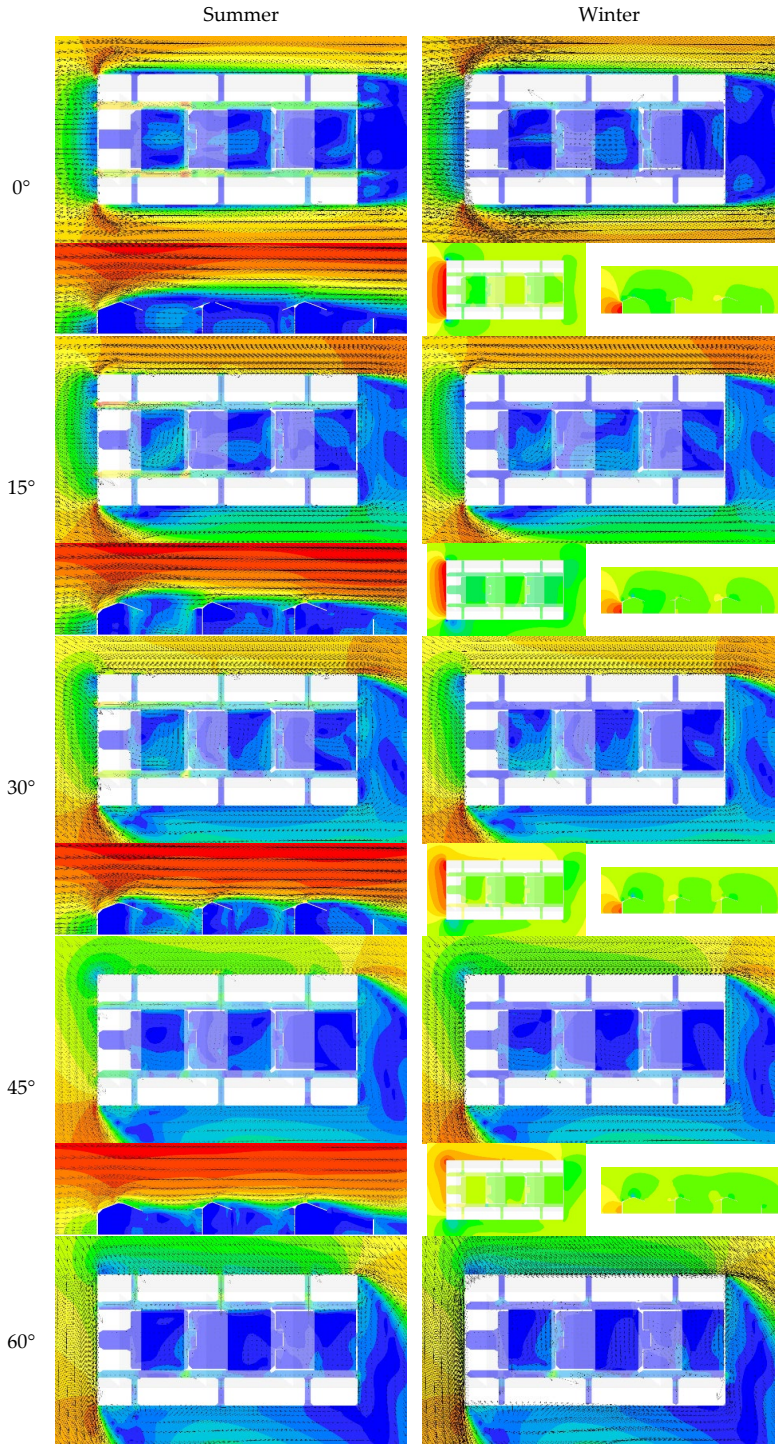


Figure 16. *Cont*.

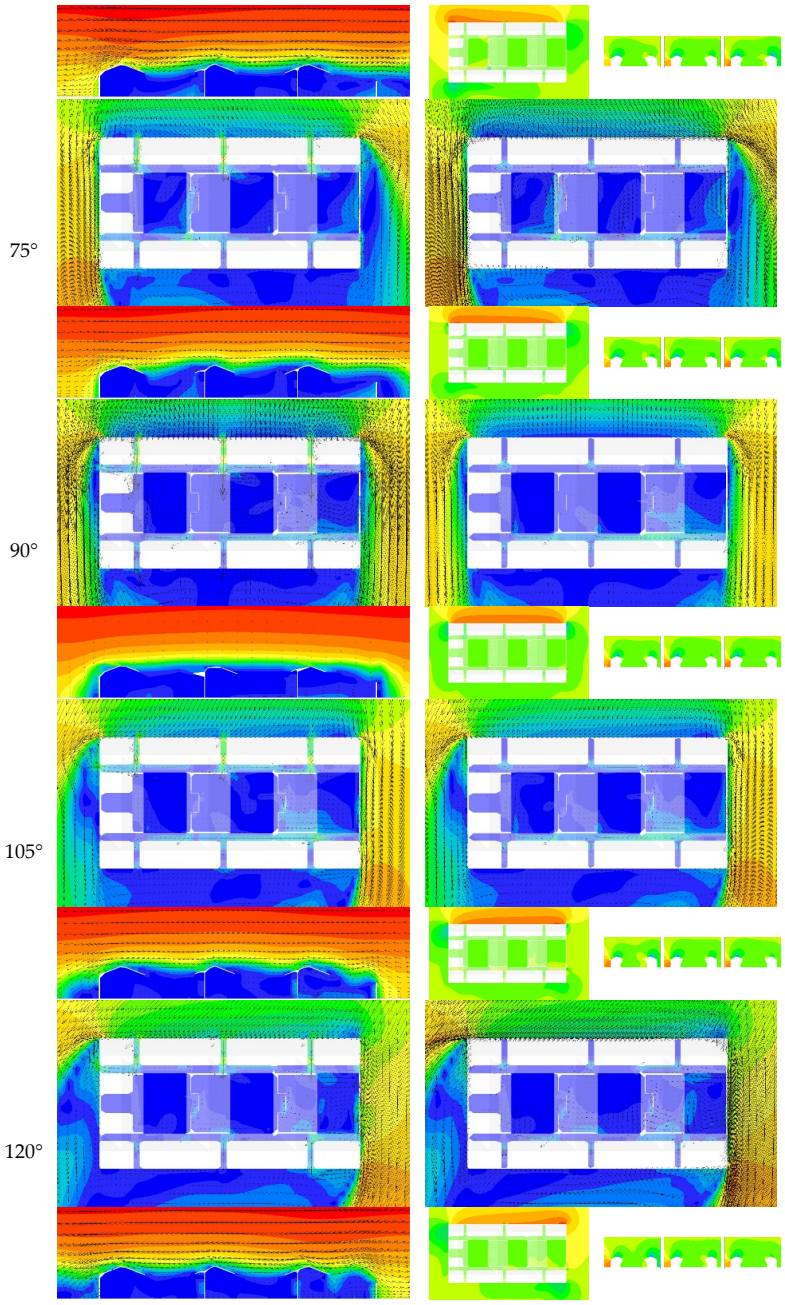


Figure 16. *Cont*.

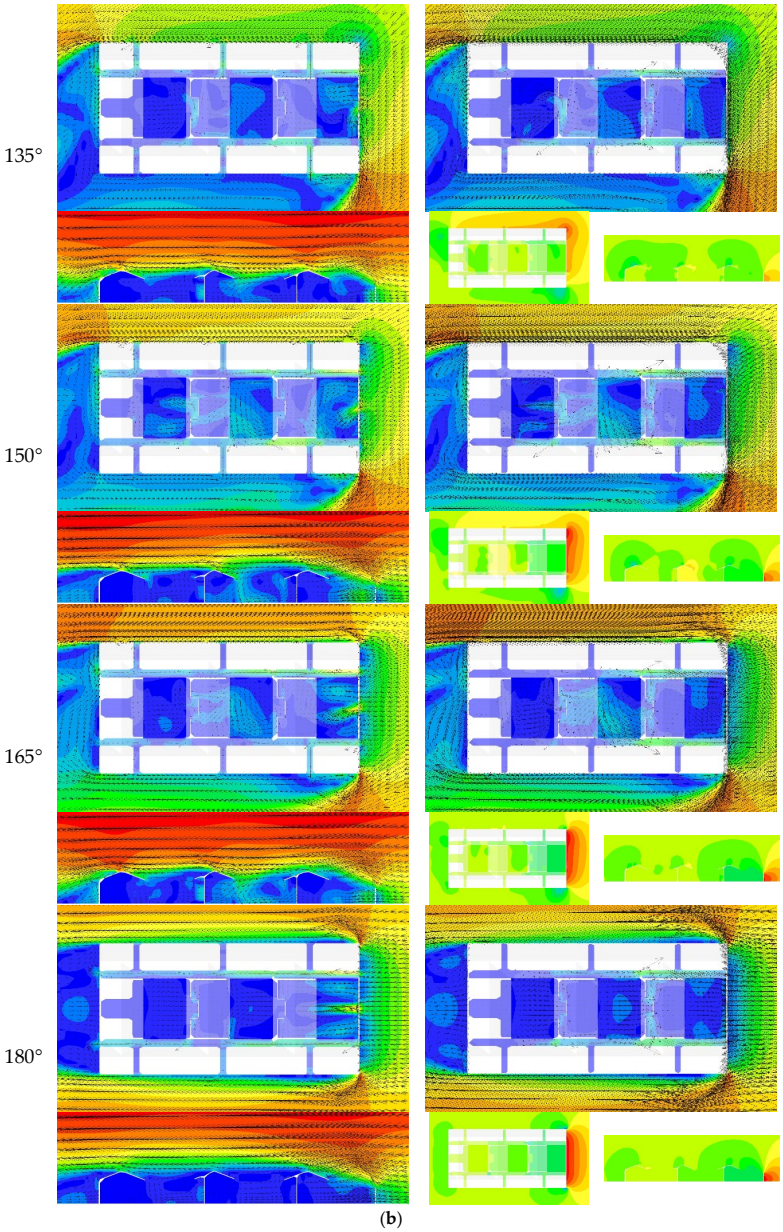


Figure 16. (**a**) Stimulation condition; (**b**) stimulation results.

Findings:

- Wind Environment Gradient and Functional Adaptability of Courtyard Layout

Simulation outcomes demonstrate a distinct "wind environment gradient" within the longitudinal three-courtyard complex, which correlates closely with its spatial hierarchy. During summer, wind velocities diminish progressively from 1.5–1.8 m/s in the first courtyard to 0.8–1.2 m/s in the second, and further to 0.5–0.7 m/s in the third; in winter, these velocities decrease from 0.8–1.0 m/s to 0.3–0.5 m/s and 0.2–0.3 m/s, respectively. This gradient is consistent with the functional zoning—public, semi-public, and private—facilitating thermal comfort and spatial adaptation. The formation of this gradient results from the sequential buffering effects of the spatial configuration: the first courtyard, aided by the stone gate and screen wall, diminishes external wind; the second, enclosed by eave galleries and the main hall, further attenuates airflow; and the third, characterized by its narrow geometry, stabilizes air movement. Collectively, these courtyards establish a gradual transition from robust to diminished airflow, reflecting the social hierarchy associated with their use.

- Dual-Optimum Intervals of Wind Direction–Orientation Angles

Results indicate that courtyard houses in hot-summer–cold-winter regions exhibit a dual-optimal interval of orientation angles for wind performance. In summer, when the building axis deviates 60–75° from the prevailing wind, courtyard airflow remains smooth (0.5–0.7 m/s) and side galleries experience comfortable breezes (0.8–1.2 m/s), meeting ventilation standards without causing discomfort. In winter, at 45–75° or 105–120°, façade wind pressure stays below 5 Pa, with mild indoor airflow (0.2–0.3 m/s) that aids air exchange while limiting heat loss. This dual-optimum pattern reflects adaptive spatial logic: in summer, prevailing northwesterly winds are guided through side galleries to enhance cross ventilation; in winter, the western façades form wind shadows to block cold drafts while eastern openings sustain light airflow. The orientation thus embodies a "summer ventilation–winter protection" strategy intrinsic to traditional courtyard design.

4.1.2. Orientation and Solar Radiation Environment

Utilizing the prototype unit model, simulations were performed to analyze solar radiation heat gain across various orientations, ranging from due south (0°) to due east (90°), in 15° increments. The simulations accounted for the summer solstice and winter solstice under the climatic conditions of Dongyang. Outcomes are depicted in Figure 17. Concerning the building components, the side chambers (B and C) are two stories, with "−1" indicating the first floor and "−2" the second floor.

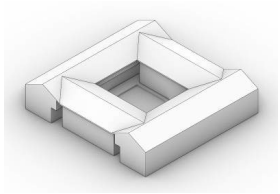
It can be observed that orientation has minimal impact on solar radiation heat gain at the ground level of the courtyard. Radiation levels remain comparatively high during the summer, approximately 4 kWh/m^2, and low during winter, around 0.65 kWh/m^2.

During the summer season, solar radiation on the axis-aligned façades (A, D) increases with deviation in orientation: between 15° and 75°, each 15° shift results in an approximate increase of 0.23 kWh/m^2 in radiation. The southern façade (D) consistently receives marginally more radiation than the northern façade (A). Conversely, on the first-floor façades of the side chambers (B, C), solar radiation diminishes with deviation: between 15° and 60°, each 15° shift causes a reduction of approximately 0.25 kWh/m^2. The eastern chamber (C) receives slightly more radiation compared to the western chamber (B).

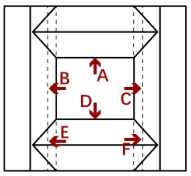
During the winter season, solar radiation on the south façade (A) diminishes with increased deviation: within the range of 15° to 90°, each 15° increment results in an approximate reduction of 0.4 kWh/m^2 in radiation. Conversely, on the western chamber (B), radiation intensifies with increased deviation: between 0° and 75°, each 15° shift correlates with a roughly 0.3 kWh/m^2 increase. On the north façade (D), radiation remains relatively constant at approximately 0.37 kWh/m^2 within the deviation range of 0° to 60° but experiences a slight increase of 0.1 kWh/m^2 per 15° between 60° and 90°. The impact of orientation on the eastern chamber (C) is comparatively minor, with radiation levels maintained around 0.37 kWh/m^2.

The variations in daily solar radiation heat gain with respect to orientation for the second-floor side chambers, the first-floor side chambers flanking the main hall, and the ground surfaces of the eave gallery are illustrated in Figure 18.

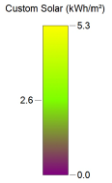
It can be observed that orientation deviations have minimal impact on the solar radiation received by the first-floor side chambers flanking the main hall. During summer, the values consistently hover around 0.9 kWh/m^2, whereas in winter, they remain approximately 0.35 kWh/m^2 for the eastern chamber and range between 0.5 and 0.8 kWh/m^2 for the western chamber.



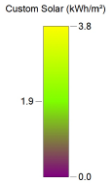
Prototype Model



Simulation Interfaces



Legend (Summer)

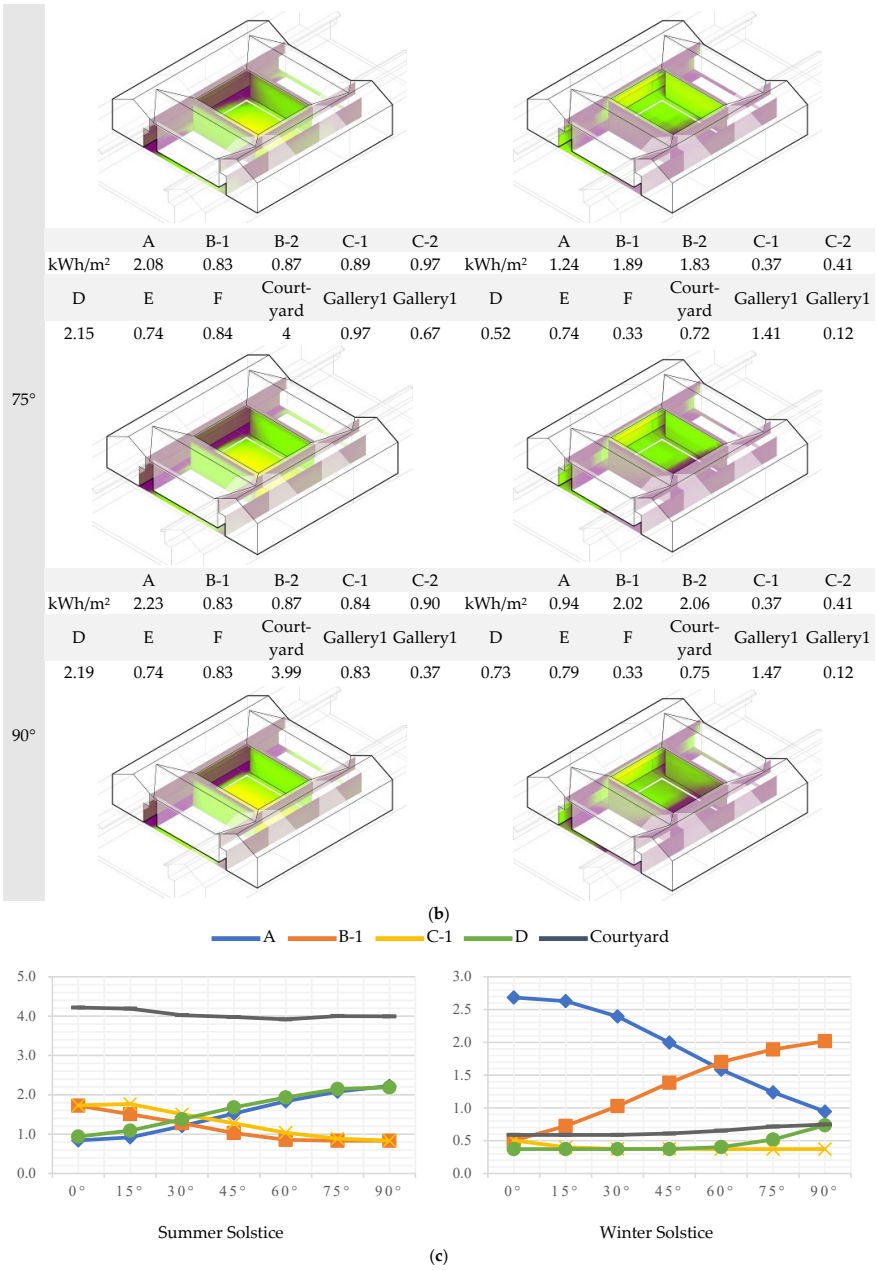


Legend (Winter)

(**a**)

	Summer Solstice						Winter Solstice				
0°		A	B-1	B-2	C-1	C-2		A	B-1	B-2	C-1	C-2
	kWh/m²	0.84	1.72	1.63	1.73	1.63	kWh/m²	2.68	0.50	0.67	0.50	0.67
	D	E	F	Court-yard	Gallery1	Gallery1	D	E	F	Court-yard	Gallery1	Gallery1
	0.94	0.82	0.82	4.22	2.14	2.32	0.37	0.49	0.49	0.59	0.32	0.33
15°		A	B-1	B-2	C-1	C-2		A	B-1	B-2	C-1	C-2
	kWh/m²	0.92	1.51	1.47	1.77	1.67	kWh/m²	2.63	0.73	0.87	0.4	0.51
	D	E	F	Court-yard	Gallery1	Gallery1	D	E	F	Court-yard	Gallery1	Gallery1
	1.09	0.91	0.8	4.19	2.11	2.19	0.37	0.53	0.43	0.59	0.55	0.17
30°		A	B-1	B-2	C-1	C-2		A	B-1	B-2	C-1	C-2
	kWh/m²	1.21	1.28	1.27	1.51	1.49	kWh/m²	2.39	1.03	1.14	0.37	0.42
	D	E	F	Court-yard	Gallery1	Gallery1	D	E	F	Court-yard	Gallery1	Gallery1
	1.38	0.97	0.87	4.02	1.98	1.86	0.37	0.56	0.36	0.59	0.81	0.13
45°		A	B-1	B-2	C-1	C-2		A	B-1	B-2	C-1	C-2
	kWh/m²	1.52	1.03	1.08	1.28	1.33	kWh/m²	2.00	1.38	1.41	0.38	0.41
	D	E	F	Court-yard	Gallery1	Gallery1	D	E	F	Court-yard	Gallery1	Gallery1
	1.68	0.93	0.91	3.98	1.73	1.52	0.37	0.59	0.33	0.61	1.07	0.13
60°		A	B-1	B-2	C-1	C-2		A	B-1	B-2	C-1	C-2
	kWh/m²	1.84	0.86	0.88	1.04	1.15	kWh/m²	1.58	1.7	1.59	0.37	0.41
	D	E	F	Court-yard	Gallery1	Gallery1	D	E	F	Court-yard	Gallery1	Gallery1
	1.93	0.81	0.89	3.92	1.47	1.10	0.40	0.66	0.33	0.65	1.29	0.13

Figure 17. *Cont.*



	A	B-1	B-2	C-1	C-2		A	B-1	B-2	C-1	C-2
kWh/m²	2.08	0.83	0.87	0.89	0.97	kWh/m²	1.24	1.89	1.83	0.37	0.41
	D	E	F	Court-yard	Gallery1	Gallery1	D	E	F	Court-yard	Gallery1	Gallery1
	2.15	0.74	0.84	4	0.97	0.67	0.52	0.74	0.33	0.72	1.41	0.12

	A	B-1	B-2	C-1	C-2		A	B-1	B-2	C-1	C-2
kWh/m²	2.23	0.83	0.87	0.84	0.90	kWh/m²	0.94	2.02	2.06	0.37	0.41
	D	E	F	Court-yard	Gallery1	Gallery1	D	E	F	Court-yard	Gallery1	Gallery1
	2.19	0.74	0.83	3.99	0.83	0.37	0.73	0.79	0.33	0.75	1.47	0.12

Figure 17. (**a**) Stimulation condition; (**b**) stimulation results; (**c**) variation in daily solar radiation heat gain of the façades with respect to orientation.

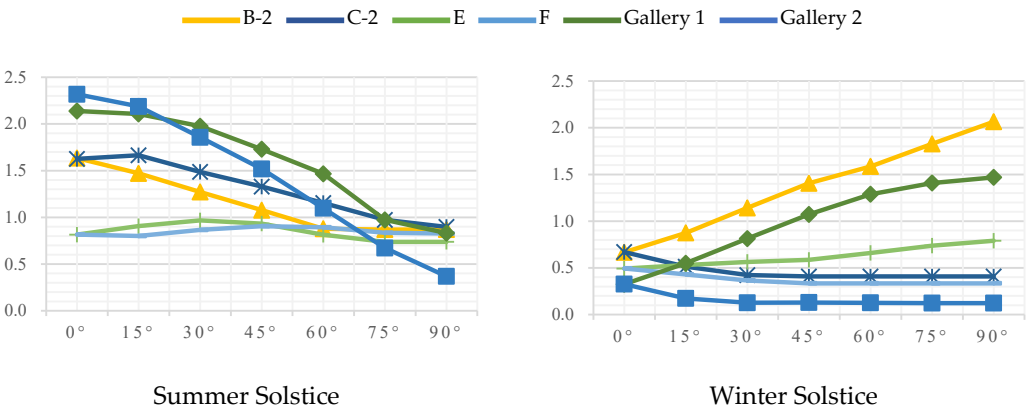


Figure 18. Variation in solar daily radiation heat gain of the façades with respect to orientation.

During the summer season, solar radiation on the façades of the side chambers located on the second floor (B, C) diminishes as the orientation deviates. Specifically, within the range of 15° to 75°, each 15° alteration results in an approximate reduction of 0.2 kWh/m^2 in radiation. It is also observed that the eastern chamber (B) receives greater solar radiation compared to the western chamber (C). Additionally, solar radiation on the ground surfaces of the east–west eave gallery declines with increasing orientation deviation, with the west eave gallery consistently registering higher levels than the east.

During the winter season, solar radiation on the second floor of the western chamber (B) and the ground surface of the western eave gallery exhibits an increase correlating with orientation deviation, at an approximate rate of 0.23 kWh/m^2 per 15°. Conversely, orientation exerts only a marginal influence on the second floor of the eastern chamber (C) and the ground surface of the eastern eave gallery.

The daily solar radiation heat gain values for each façade and surface are summarized in Table 6.

Table 6. Daily solar radiation heat gain values for each façade.

	Summer Solstice							**Winter Solstice**						
	0°	**15°**	**30°**	**45°**	**60°**	**75°**	**90°**	**0°**	**15°**	**30°**	**45°**	**60°**	**75°**	**90°**
A	2.68	2.63	2.39	2.00	1.58	1.24	0.94	0.84	0.92	1.21	1.52	1.84	2.08	2.23
B-1	0.50	0.73	1.03	1.38	1.70	1.89	2.02	1.72	1.51	1.28	1.03	0.86	0.83	0.83
B-2	0.67	0.87	1.14	1.41	1.59	1.83	2.06	1.63	1.47	1.27	1.08	0.88	0.87	0.87
C-1	0.50	0.40	0.37	0.38	0.37	0.37	0.37	1.73	1.77	1.51	1.28	1.04	0.89	0.84
C-2	0.67	0.51	0.42	0.41	0.41	0.41	0.41	1.63	1.67	1.49	1.33	1.15	0.97	0.90
D	0.37	0.37	0.37	0.37	0.40	0.52	0.73	0.94	1.09	1.38	1.68	1.93	2.15	2.19
Total	5.40	5.51	5.73	5.94	6.05	6.26	6.54	8.50	8.42	8.13	7.92	7.69	7.79	7.85

In summary, during the summer, an orientation ranging from 0° to 15° is advantageous for minimizing solar heat gain on buildings aligned with the axis, whereas an orientation between 60° and 90° is beneficial for the side chambers. When considering all façades collectively, a deviation of 60° yields the lowest overall solar heat gain, while a deviation of 30° offers a more balanced distribution across the building surfaces.

During the winter season, an orientation ranging from 0° to 15° proves advantageous for maximizing solar heat gain on axis-aligned structures, whereas an orientation between 75° and 90° is preferable for the western chamber. The overall heat gain across all façades reaches its maximum at 90°, while an orientation of 60° again results in a more uniform distribution.

Given the hot-summer and cold-winter climate of Zhejiang, it is advisable to minimize solar heat gain on courtyards and building façades during the summer months while optimizing it during the winter. Accordingly, an orientation of 0–15° is deemed ideal for axis-aligned structures to facilitate summer cooling and winter heating. Conversely, an orientation of 30–60° ensures a more equitable distribution of solar radiation across main halls, side chambers, and both stories.

4.2. Courtyard

4.2.1. Courtyard Proportions and Wind Environment

Utilizing the prototype model of the Thirteen-Bay House, simulations were performed with the distance between the two side chambers held constant, while the courtyard length–width ratio was varied from 1:0.5 to 1:1. The input wind speed was established at 2.7 m/s, reflecting the annual average in Jinhua. The results are presented in Figure 19.

Simulation results demonstrate that the courtyard aspect ratio exerts a "nonlinear inflection point" effect on ventilation efficiency. When the aspect ratio is less than 1:0.7, and under conditions where wind direction is not perpendicular to orientation (e.g., 0° or 45°), courtyard wind speed increases significantly as the aspect ratio decreases (with each 0.1 reduction corresponding to a 0.3–0.4 m/s increase). However, when the aspect ratio falls below 1:0.6, the rate of growth slows (only 0.1–0.2 m/s per 0.1 reduction), and air stagnation zones (wind speed < 0.3 m/s) tend to form at both ends of the courtyard. Conversely, when the aspect ratio exceeds 1:0.8, winter wind speeds within the courtyard generally remain below 0.5 m/s, producing a pronounced thermal buffering effect (courtyard air temperature 1–2 °C higher than open-air conditions), though summer ventilation efficiency decreases by 20–25%.

The causes of this inflection point can be articulated as follows: when the aspect ratio is excessively small (<1:0.6), the narrow-channel effect of the flanking building façades reaches saturation, thereby restricting airflow diffusion and inducing localized stagnation. Conversely, when the aspect ratio is excessively large (>1:0.8), the guiding influence of the façades on airflow diminishes: in summer, prevailing winds are insufficient to produce effective cross-courtyard ventilation; in winter, the reduced spatial confinement facilitates the accumulation of warm air, thereby forming a stable thermal buffer layer. Coupled with field data obtained from the Lu residence (Courtyard A width-to-depth ratio = 2.16, with winter temperatures ranging from 0.5 to 0.8 °C higher than those of Courtyard C), it can be inferred that the traditional courtyard's preference for a "narrow-elongated" configuration (aspect ratio 1:0.5–1:0.7) directly responds to the hot-summer–cold-winter climatic requirement of "summer ventilation prioritized, winter insulation supplementary." The design of courtyard aspect ratios consistently fluctuates around this ventilation efficiency inflection point, rather than adopting a uniformly elongated morphology.

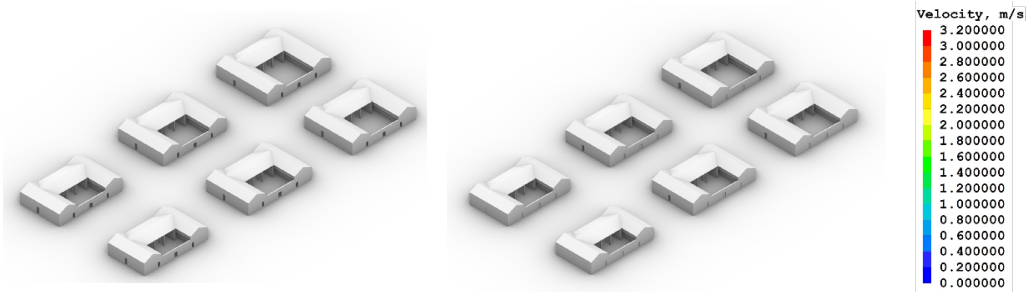
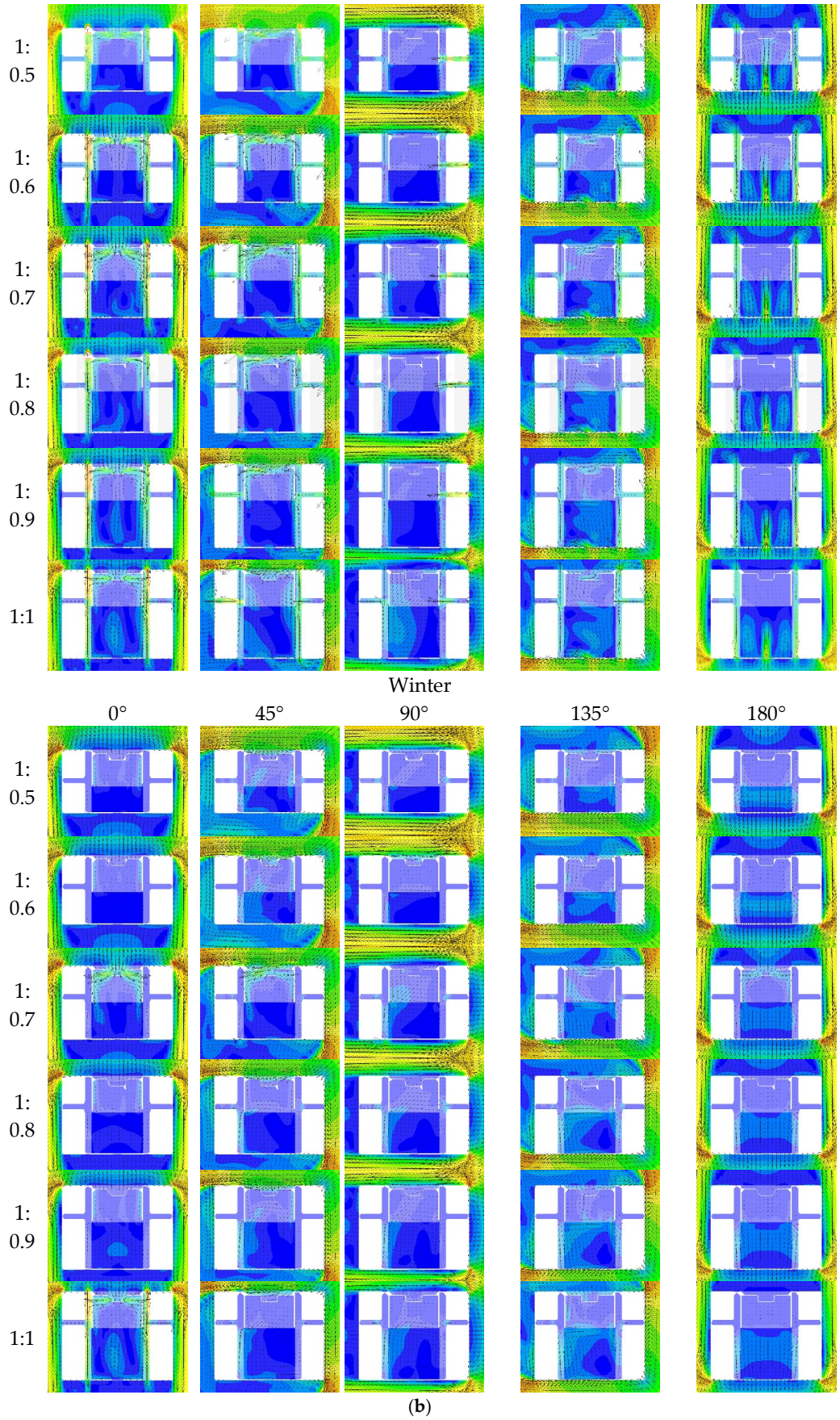


Figure 19. *Cont.*



(**b**)

Figure 19. (**a**) Stimulation condition; (**b**) stimulation results.

4.2.2. Courtyard Proportions and Thermal Environment

Field measurements demonstrated that façade solar heat gain correlates with the height–width ratio of the courtyard along the solar exposure direction. Consequently, simulations were conducted utilizing the prototype unit model oriented due north, with the distance between side chambers set at one unit. The height-to-depth ratio of the main building and courtyard was varied among 1:0.5, 1:1, 1:1.5, 1:2, 1:2.5, and 1:3. Solar radiation was simulated for the summer and winter solstices under the climatic conditions of Dongyang. The results are presented in Figure 20.

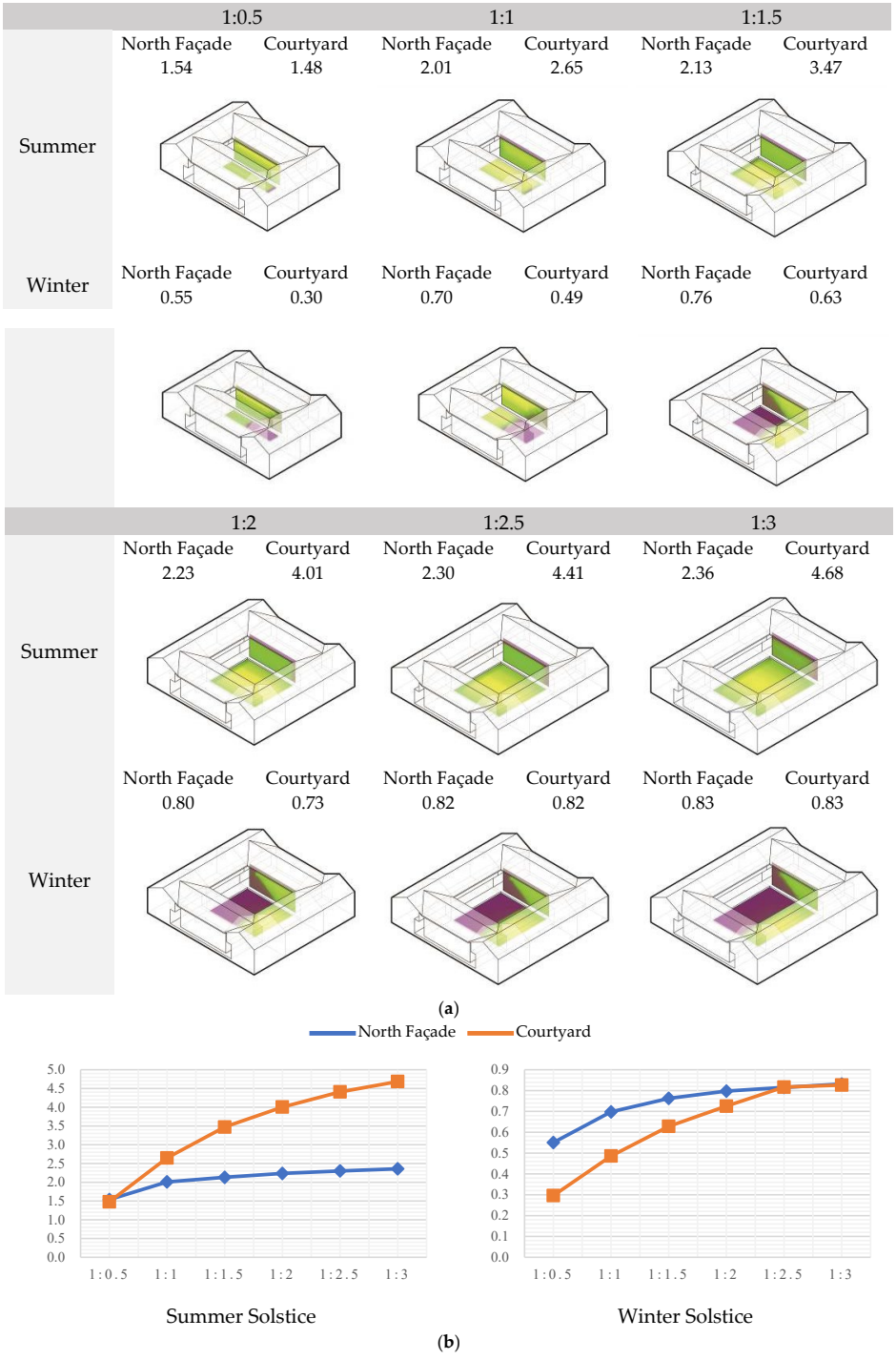


Figure 20. (**a**) Stimulation results; (**b**) variation in daily solar radiation heat gain of the façades.

During the winter season, when the height–width ratio falls below 1:2.5, both the surfaces of the courtyard ground and the north-facing façades receive optimal solar radiation. Conversely, in the summer months, solar radiation at ground level increases as the ratio decreases, while the impact on north-facing façades remains negligible. Overall, a courtyard height–width ratio of less than 1:2.5 promotes enhanced solar heat gain during winter with minimal adverse effects on summer conditions, thereby improving climatic adaptability throughout the year.

4.3. Eave Gallery

The configuration of the Thirteen-Bay House, distinguished by two-story side chambers integrated with a continuous ground-floor eave gallery, inherently creates wind channels. As evidenced in prior wind environment simulations, ventilation within the eave galleries surpasses that of the courtyards: wind speeds in the eave galleries are 3–5 times greater than those within the courtyards, establishing them as the principal ventilation pathway during summer.

Eave galleries exert an indirect influence on the thermal environment through their shading effects on facades. The Thirteen-Bay House exhibits a diverse array and considerable number of eave spaces, including projecting eaves, front galleries, and cloisters. These components function as vital shading devices during the summer months. Conversely, in winter, when the solar altitude angle is lower, they permit increased solar radiation to penetrate the facades. In Zhejiang, the eave depths vary between 600 and 2700 mm, outer eave heights range from 3000 to 4000 mm, and the slopes average approximately 25°.

For the simulations, the inner eave height was established as 4.5 m, while the eave depths were varied at 0, 600, 900, 1200, 1500, 1800, 2100, 2400, and 2700 mm. Solar radiation heat gain on the façades beneath the eaves was subsequently simulated under each condition for the entire day during both the summer solstice and winter solstice. Results are illustrated in Figure 21.

To assess the shading impact of the eave galleries on solar radiation, the ratio of solar radiation under each condition to that without eaves was calculated, as demonstrated in Table 7.

Table 7. Daily solar radiation heat gain values for each façade.

	600	900	1200	1500	1800	2100	2400	2700
Summer	81%	73%	67%	62%	57%	54%	50%	48%
Winter	92%	89%	85%	81%	78%	75%	73%	70%
Summer /Winter	88%	82%	79%	77%	73%	72%	68%	69%

During the summer season, when the eave depth varies from 0 to 900 mm, the shading efficacy increases markedly with depth; between 900 and 1800 mm, each additional 100 mm of depth diminishes solar radiation by approximately 5%. Beyond 1800 mm, the rate of reduction in solar radiation decreases. Once the eave depth surpasses 900 mm, simulation results demonstrate the absence of direct solar exposure (indicated by the lack of yellow zones in the diagrams), signifying that façades are entirely shielded from direct sunlight during summer.

During the winter season, an increase of 100 mm in eave depth results in an approximate reduction of 3% in solar radiation. When the eave depth surpasses 1500 mm, the solar heat gain diminishes by in excess of 20%.

At an eave depth of 2400 mm, the ratio of summer reduction to winter retention attains its peak, signifying that summer shading efficacy is optimized while preserving the proportional heat gain through the winter façade.

Taking into account both summer shading and winter solar gain, an eave depth ranging from 900 to 1500 mm is deemed optimal: during summer, it provides effective shading, decreasing heat gain by approximately 35%, whereas in winter, it minimally reduces solar radiation by about 15%. Considering the increased requirement for shading in the summer, an eave depth of approximately 2400 mm may be deemed suitable.

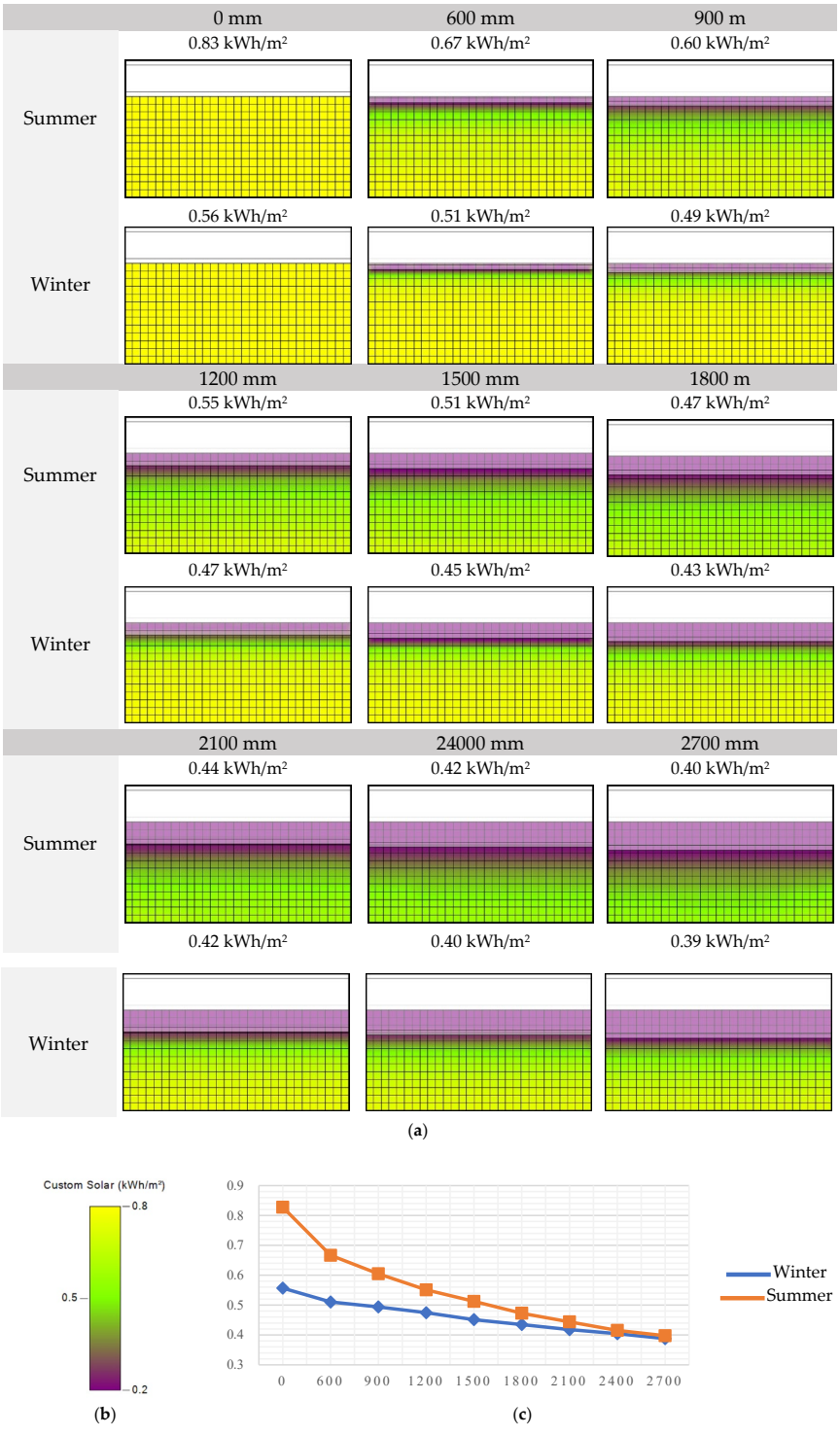


Figure 21. (**a**) Stimulation results; (**b**) legend for the simulation results; (**c**) variation in daily solar radiation heat gain of the façades with different eave depths.

5. Discussion

5.1. Key Findings

- Synergistic Regulation Mechanism of Wind–Light–Thermal Interactions in Transitional Spaces: During winter, the northern interface of the courtyard functions as the primary heat-gain zone within the building complex, with radiation heat gains in transitional spaces exceeding indoor levels by 15–20%. The west eaves of the courtyard diminish the velocity of prevailing winter westerlies by over 60%, effectively preventing cold air ingress. Courtyard paved surfaces store thermal energy, maintaining the near-ground air temperature 1–2 °C above the meteorological air temperature. Passage halls regulate airflow through the opening and closing of aligned doors, maintaining wind speeds below 1 m/s, thus ensuring thermal comfort and preserving indoor air quality.
- Optimal Orientation Thresholds of the Ensemble: For axial buildings, the optimal orientation is 15° east or west of due south, maximizing winter heat gain and summer shading. For the ensemble as a whole, orientations 30–60° east or west of south balance solar heat gain across main halls, side chambers, and both floors. The optimal angle between the building axis and the prevailing wind direction is 60–75°.
  Considering the climatic variations across different areas of Jinhua, comprehensive simulation results were utilized to determine the optimal building orientations for each region. For Jinhua City, an orientation of 30–45° east of south is recommended to balance summer ventilation and winter heat gain. In Lanxi, an orientation of 30–60° east of south aligns with the prevailing wind direction and compensates for limited sunshine. For Yongkang, an orientation of 30–60° east of south meets the shading requirements of warm zones and enhances winter heat gain while accommodating prevailing winds. In Wuyi, an orientation of 30–45° east of south provides a balance between north–south solar gain and ventilation efficiency. For Pujiang, an orientation of 45–60° east of south aligns with the prevailing wind angle and supports winter heat gain in the colder northern area. In Yiwu, an orientation of 30–45° east of south ensures adequate solar gain while forming an effective ventilation angle with northerly winds. For Dongyang, an orientation of 30–45° west of south helps avoid direct northwesterly winds while balancing winter heat gain and summer ventilation.
- Optimal Thresholds of Courtyard Proportions: When the courtyard height-to-width ratio is less than or equal to 1:2.5, the winter solar radiation heat gain on the ground and north façade is maximized, while maintaining limited impact on summer conditions. A smaller ratio of the "side-chamber spacing/axial-building distance" results in higher courtyard temperatures, with elongated courtyards being more advantageous for winter heat retention. Length-to-width ratios ranging from 1:0.5 to 1:0.7 produce optimal wind environments.
- Climatic Response of Eave Galleries: An eave depth of 900–1500 mm establishes a "winter–summer balance zone," mitigating summer façade heat gain by approximately 35% while decreasing winter heat gain by only 15%. In regions where summer shading demand takes precedence, such as areas with extended hot seasons, an eave depth of approximately 2400 mm is deemed optimal, effectively reducing summer heat gain by fifty percent.
- Spatial Hierarchy and Thermal Stability: The thermal stability of a building is determined by its position within the ensemble: interior buildings (e.g., Leshoutang Hall) cool more slowly at night and remain 1–2 °C warmer than edge buildings (e.g., Gatehouse), making them better suited for residential use. A higher proportion of façade area facing the courtyard corresponds to lower thermal stability. Differences in thermal performance between halls and side chambers align with the functional

distinction between "activity" and "residence," embodying the design wisdom of traditional courtyard houses where "form adapts to function."

5.2. Application in Design

This study emphasizes design guidelines that address the dual objectives of "morphological continuity" and "climatic adaptability" in traditional courtyard houses situated in hot-summer cold-winter regions. The insights gained were implemented in the project adjacent to Xu Zhen Er Gong Ancestral Hall heritage site. The site, located in Yongkang, Jinhua, encompasses the construction of two new courtyard-style guesthouses within the designated protected boundary. As the area is classified as a historical conservation district, the new structures were mandated to preserve traditional spatial configurations. Accordingly, the design incorporated the optimal transitional space parameters derived from this research, in compliance with heritage protection regulations.

The prototype of the "Thirteen-Bay House" was adopted, and, in accordance with site conditions, two courtyards were arranged. The building ensemble features a frontage of 29,720 mm (Figure 22a). Each courtyard is encircled by eave galleries, with passageways connecting the main hall and side chambers, thereby continuing the "non-sealed regulation" mechanism of the Lu Residence.

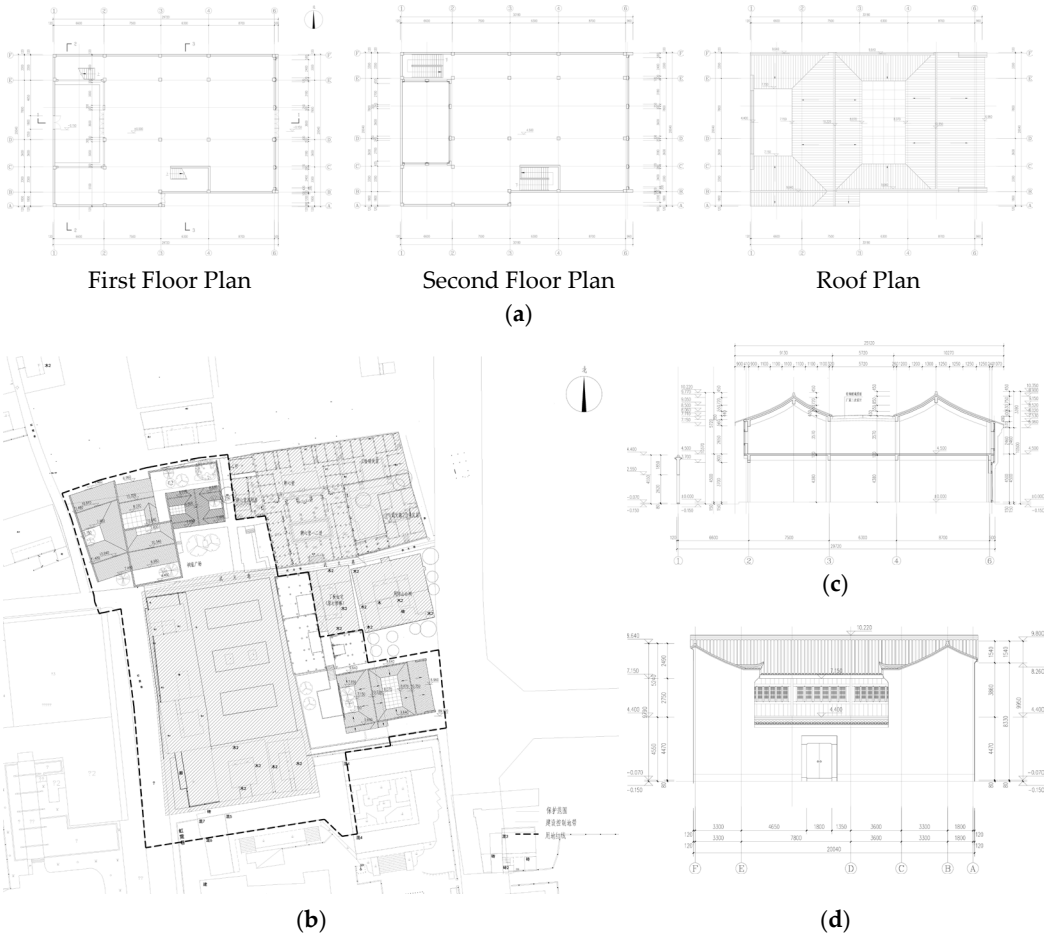


Figure 22. (**a**) Plan; (**b**) site plan; (**c**) section; (**d**) west elevation.

In accordance with the study's findings on balancing "winter wind protection and heat gain" with "summer ventilation and shading," key geometric parameters were quantitatively adjusted. In traditional Chinese residential architecture, orientation was frequently determined by the natural environment—such as rivers and mountains—and was culturally directed by the principles of feng shui. In established urban streets, newly developed build-

ing complexes typically conform to the prevailing street orientation. While adhering to this culturally embedded constraint, our objective is to align the design as closely as possible with the climate-optimized solution, thereby facilitating a comparison between practical implementation and the theoretical optimum. Given the prevailing north-northeasterly winds in Yongkang, a 60–75° wind-axis angle was identified as optimal, and when combined with solar gain considerations, the theoretical orientation was 30° east of south. Under given site constraints, the final orientation was set at 18° east of south (Figure 22b). For courtyard dimensions, the frontage was 12,340 mm and depth 7600 mm, yielding a length-to-width ratio of 1:0.6—within the optimal range of 1:0.5–1:0.7 for wind environment. The height-to-width ratio was 1:2—within the $\leq$1:2.5 threshold for thermal performance (eave height of main hall 4500 mm, courtyard depth 7600 mm, Figure 22c). Eave depth on the first floor was uniformly set at 1200 mm (Figure 22d), within the recommended "900–1500 mm winter–summer balance zone."

Based on conclusions regarding the thermal differences of façade materials, traditional material systems were retained with optimized construction for enhanced passive regulation. Lower walls utilized 300 mm brick bases, consistent with the thickness of the Lu Residence, and were complemented by 40 mm timber lattice panels arranged above, as indicated by field survey data. A whitewashed layer was applied beneath the windowsills, in accordance with the practice observed on the Gatehouse south façade, resulting in a reduction of solar absorption during summer by 20%. A hard-gable roof, identical to the side chambers of the Lu Residence, was adopted with a 25° pitch and covered using traditional tiles, thereby improving insulation during winter and providing shading during summer. The heat transfer coefficient of the roof was maintained below 0.5 W/(m^2·K).

Post-construction, field surveys were conducted during winter (February 2025) to validate the results. On clear winter days (outdoor temperatures ranging from 2 to 9 °C), eave gallery temperatures on the northern side ranged from 12 to 14 °C, exceeding outdoor temperatures by 3 to 4 °C. Meanwhile, indoor rooms (side chambers) maintained temperatures between 14.5 and 16 °C, fulfilling residential comfort standards. The prevailing westerly winds (external velocity approximately 4 m/s) were mitigated to velocities between 1.0 and 1.2 m/s within the courtyard following adjustments involving eave galleries and openings. Passage hall airflow was measured at 0.8 m/s, effectively preventing cold drafts.

In summary, the Xu Zhen Er Gong Ancestral Hall project illustrates that by incorporating optimized dimensions derived from the climate-adaptive prototype of the "Thirteen-Bay House" during the initial design phase, built environments can be enhanced while preserving cultural continuity. This affirms that climate adaptability strategies for transitional spaces in traditional courtyard residences can be quantitatively adapted for modern application, establishing a replicable model suitable for hot-summer cold-winter regions.

5.3. Innovations

This research extends beyond the traditional "settlement–interior" dual framework by focusing on transitional spaces—including courtyards, eave galleries, and passage halls—as the primary subjects of investigation. Their function in mediating "outdoor–indoor" environments was quantitatively examined, revealing the winter synergistic effects of "west eave gallery wind protection, north façade heat gain, and courtyard heat storage." Critical thresholds, such as eave depth and courtyard height-to-width ratio, were identified, offering scientific delineations for the design of transitional spaces.

A multi-parameter coupled simulation method integrating summer and winter conditions was developed. Addressing the limitations of previous studies that focus either on summer ventilation or winter insulation, this research combined both requirements—"blocking cold winds in winter, guiding cool breezes in summer." By applying multi-

software collaboration, wind–light–thermal interactions were simulated in tandem, rather than as isolated variables, more accurately reflecting real climatic regulation.

The practical application of these findings was demonstrated through integration into the Xu Zhen Er Gong Ancestral Hall guesthouse project. Passive green design strategies were implemented from the design stage, establishing a matching mechanism between regional climate and the geometric parameters of transitional spaces, thereby providing a viable pathway for the scientific advancement of traditional architectural forms.

5.4. Limitations and Outlook

Despite systematically uncovering the climatic adaptability mechanisms of transitional spaces in the Lu Residence, this study presents several limitations.

Survey limitations include conducting field measurements exclusively during the winter season, without encompassing summer or transitional periods, thereby precluding the ability to accurately represent year-round climatic regulation. In future research, it will be necessary to incorporate climate survey data from the warmest month. In comparison with the winter measurement protocol, the summer survey necessitates the deployment of additional temperature and humidity sensors positioned beneath the eaves to ascertain their efficacy in summer heat insulation. To evaluate the wind channeling effect within the corridors during the summer, multiple measurement stations should be strategically placed along the corridors as well as within the rooms to monitor variations in wind speed throughout the day. Additionally, site constraints and limited manpower resulted in insufficient data collection from simultaneous multi-point, long-duration monitoring, which particularly diminished the analytical robustness of the wind environment findings. In future research, we also consider employing alternative turbulence models to assess sensitivity to local wind effects and to validate the simulation outcomes.

Computational simulations inherently simplify various real-world factors. Specifically, the deterioration of materials due to aging—such as timber panels and brick walls—was not accounted for, nor were human behavioral variables—such as door and window usage patterns and occupancy differences—that impact the microclimate. Consequently, discrepancies exist between the simulated environments and actual residential settings, and these factors were not extensively analyzed, leaving room for future research.

A brief post-construction survey and environmental data collection were conducted following the completion of the building. However, as the project has not yet been commissioned and the space remains unoccupied by guests, user feedback is currently unavailable. A follow-up assessment of passengers' actual comfort experiences will be carried out once the facility becomes operational, with the purpose of further evaluating the efficacy of the proposed design strategy. Furthermore, this study does not encompass a discussion on the selection of interface materials or the impact of material aging on the built environment, which warrants additional in-depth investigation.

6. Conclusions

The climate adaptability strategies of transitional spaces within the "Thirteen-Bay House" typology in the Jinhua region can be summarized as follows.

At the ensemble scale, the optimal orientation for axial buildings lies between 15° west of south and 15° east of south, while the general orientation for all buildings should fall within 30–60° east or west of south, or 45–60° relative to the prevailing annual wind direction. This configuration maximizes both solar access and ventilation efficiency throughout the year.

At the courtyard level, geometric proportions are instrumental in attaining climatic equilibrium. The ideal height-to-width ratio should not surpass 1:2.5, whereas the length-to-

width ratio is most appropriately maintained within the range of 1:0.5 to 1:0.7. Concerning the layout, it is noted that the first courtyard typically encounters higher wind velocities; consequently, the installation of a screen wall on the outer side or adjacent to the side entrances can effectively mitigate wind effects and enhance occupant comfort.

Regarding the building scale, thermal stability can be enhanced by situating the primary functional spaces within the interior zone of the complex. Increasing the proportion of façades facing the courtyard, relative to the total envelope area, improves heat retention and radiation exchange. Furthermore, a higher ratio of floor height to depth facilitates improved indoor temperature stability.

Regarding usage patterns, axial halls are more comfortable during daytime hours and are therefore appropriate for hosting receptions and public gatherings. In contrast, side chambers tend to preserve more stable temperatures during nighttime, rendering them suitable for accommodation purposes.

Regarding the eaves, the side-chamber galleries function as natural ventilation pathways, facilitating advantageous airflow beneath both sides of the roof. The optimal eaves depth, which balances winter heat gain with summer shading, is typically between 900–1500 mm. Conversely, for shading-dominant configurations, a depth of approximately 2400 mm is advised.

Overall, these strategies collectively demonstrate how traditional architectural forms achieve seasonal adaptability through spatial organization, geometric proportioning, and transitional-space optimization, providing valuable references for contemporary green building design in regions characterized by hot summers and cold winters.

Within the hot-summer and cold-winter zone of China's Yangtze River Delta, comprising Zhejiang Province, southern Jiangsu, southern Anhui, Shanghai, northeastern Jiangxi, and northern Fujian, the climatic characteristics and thermal requirements of buildings align with those of Jinhua. Specifically, insulation is necessary during winter, while shading and ventilation are crucial in summer. Historically, vernacular dwellings in these regions have been significantly influenced by Hui-style architecture, exhibiting similar spatial typologies and abundant intermediary spaces. Consequently, the findings of this study may be extended to courtyard-style buildings in these areas, especially those situated in plains and shallow hilly regions of small- and medium-sized cities and towns, where building density remains moderate and extreme topographical or climatic conditions—such as deep mountain terrains or regions prone to strong winds—are absent.

When implementing these findings in practice, several limitations must be taken into account:

- Differences in climatic subdivisions: The northern regions of the Yangtze River Delta endure colder winters, thereby necessitating enhanced insulation for northern façades and improved heat retention within courtyards. Conversely, the southern areas are characterized by higher temperatures and increased humidity during summer, requiring deeper eaves and broader ventilation corridors, which are not entirely addressed by the original design.
- The complexity of prevailing winds: In certain cities within the Yangtze River Delta, the predominant wind direction exhibits substantial variation across different seasons. A fixed building orientation may not sufficiently accommodate both summer and winter wind patterns; therefore, the incorporation of adjustable ventilation components is advised.
- Topographic and density constraints: In mountainous cities, substantial elevation variations pose challenges to maintaining consistent courtyard proportions and orientations. In densely populated urban centers, elongated courtyard configurations and spacing requirements frequently prove impractical, potentially undermining thermal stability and wind performance.

- Limitations of functional adaptation: Contemporary courtyard complexes may integrate commercial or office functionalities, thereby modifying the initial thermal performance distribution established for "activity–residence" configurations. The conventional spatial logic cannot be directly employed without functional modifications.

Author Contributions: Conceptualization, J.W.; methodology, J.W.; software, J.W.; validation, J.W. and H.L.; formal analysis, H.L.; investigation, J.W.; resources, L.B.; data curation, J.W.; writing—original draft preparation, J.W. and H.L.; writing—review and editing, H.L. and L.B.; visualization, J.W.; supervision, L.B.; project administration, L.B.; funding acquisition, L.B. All authors have read and agreed to the published version of the manuscript.

Funding: This research was funded by National Key R&D Program of China during the "13th Five-Year Plan" period under the project titled "Study on the Green Design Concepts, Methods and Their Inheritance in Traditional Architectural Culture of Economically Developed Regions" (Grant No. 2017YFC0702501).

Data Availability Statement: The original contributions presented in this study are included in the article. Further inquiries can be directed to the corresponding author.

Conflicts of Interest: Authors Jiaqi Wang and Huijie Liu were employed by the company Zhejiang Province Institute of Architectural Design and Research Co., Ltd. The remaining authors declare that the research was conducted in the absence of any commercial or financial relationships that could be construed as a potential conflict of interest.

References

1. *JGJ 134-2010*; Design Standard for Energy Efficiency of Residential Buildings in Hot Summer and Cold Winter Zone. China Architecture & Building Press: Beijing, China, 2010.
2. Ministry of Housing and Urban-Rural Development of the People's Republic of China. *Complete Collection of Chinese Traditional Residential Types*; China Architecture & Building Press: Beijing, China, 2014.
3. Tang, G. *Traditional Architecture in Lingnan's Hot-Humid Climate*; China Architecture & Building Press: Beijing, China, 2005.
4. Editorial Committee. *Analysis and Inheritance of Traditional Chinese Architecture: Tianjin, Liaoning, Guangdong, Jiangsu, Anhui, and Zhejiang Volumes*; China Architecture & Building Press: Beijing, China, 2017.
5. Lu, Y. (Ed.) *Chinese Vernacular Architecture*; South China University of Technology Press: Guangzhou, China, 2003.
6. Sun, D. *Studies on Chinese Vernacular Architecture*; China Architecture & Building Press: Beijing, China, 2004.
7. Wang, G.; Cui, X.; Song, W.; Hao, Y. Spatial Climate Adaptation Characteristics and Optimization Strategies of Traditional Residential Courtyards in Cold Locations: A Case Study of Xiaoyi Ancient City in Shanxi Province, China. *Buildings* **2025**, *15*, 1659. [CrossRef]
8. Yao, G.; Han, D.; Zhang, L.; Duan, Z. The Thermal Performance of Chinese Vernacular Skywell Dwellings. *Adv. Civ. Eng.* **2021**, *2021*, 6666701. [CrossRef]
9. Huang, Z.; Yu, M.; Zheng, L.; Gong, C.; Wu, Z. One-year Field Study on Indoor Environment of Huizhou Traditional Vernacular Dwellings in China. *Procedia Eng.* **2017**, *205*, 1316–1322. [CrossRef]
10. Martinelli, L.; Matzarakis, A. Influence of height/width proportions on the thermal comfort of court-yard typology for ltalian climate zones. *Sustain. Cities Soc.* **2017**, *29*, 97–106. [CrossRef]
11. Zhao, Y.; Li, K.; Han, M.; Xiong, J.; Zhang, Y. Natural ventilation in building buffer spaces of traditional Qiang dwellings: Field study in western China. *Buildings* **2025**, *15*, 794. [CrossRef]
12. Sun, Q.Q.; Luo, Z.X.; Bai, L.J. The impact of internal courtyard configuration on thermal performance of long strip houses. *Buildings* **2023**, *13*, 371. [CrossRef]
13. Gou, S.; Li, Z.; Zhao, Q.; Nik, V.M.; Scartezzini, J.L. Climate responsive strategies of traditional dwellings located in an ancient village in hot summer and cold winter region of China. *Build. Environ.* **2015**, *86*, 151–165. [CrossRef]
14. Darvish, A.; Eghbali, G.; Eghbalic, S.R. Tree-con-figuration and species effects on the indoor and outdoor thermal condition and energy performance of courtyard buildings. *Urban Clim.* **2021**, *37*, 100861. [CrossRef]
15. Wang, Z.; Huang, T.; Wang, Y.; Dai, S.; Zeng, Y.; Chen, J.; Tang, F. Evaluation of the Impact of Courtyard Layout on Wind Effects on Coastal Traditional Settlements. *Land* **2024**, *13*, 1813. [CrossRef]
16. Muhy Al-din, S.; Jega, A. Implication of shading passive strategies in buildings of hot and humid climates for energy optimization: Lessons from vernacular dwellings in Nigeria. *J. Salutog. Arch.* **2023**, *2*, 50–69. [CrossRef]

17. Chen, J.; Tao, Z. Study on Region Adaptability of Xiguan Grand House. *Huazhong Archit.* **2016**, *34*, 7–10. [CrossRef]
18. Pan, W.; Cheng, B. Research on the Influence of the Parameters of the "AO-Shaped" Skywell of Traditional Huizhou Residential Houses on the Indoor Wind Environment. *Buildings* **2025**, *15*, 2713. [CrossRef]
19. Hao, S.; Yu, C.; Xu, Y.; Song, Y. The Effects of Courtyards on the Thermal Performance of a Vernacular House in a Hot-Summer and Cold-Winter Climate. *Energies* **2019**, *12*, 1042. [CrossRef]
20. Chen, X. Thermal Environment Regulation Mechanism and Optimization Design of Patios in Huizhou Dwellings. Ph.D. Thesis, Anhui University of Technology, Ma'anshan, China, 2020.
21. Rodriguez-Algeciras, J.; Tablada, A.; Chaos-Yeras, M.; De la Paz, G.; Matzarakis, A. Influence of aspect ratio and orientation on large courtyard thermal conditions in the historical center of Camaguiey-Cuba. *Renew. Energy* **2018**, *125*, 840–856. [CrossRef]
22. Fabbri, K.; Antonini, E.; Marchi, L. Sun-Shading Sails in Courtyards: An Italian Case Study with RayMan. *Sustainability* **2023**, *15*, 13033. [CrossRef]
23. Abdallah, A.S.H.; Mahmoud, R.M.A.; Ragab, A.; Gomaa, M.M. A Multi-Objective Optimization Method for Enhancing Outdoor Environmental Quality in University Courtyards in Hot Arid Climates. *Buildings* **2025**, *15*, 3140. [CrossRef]
24. Cao, P.; Li, T. Optimization Study of Outdoor Activity Space Wind Environment in Residential Areas Based on Spatial Syntax and Computational Fluid Dynamics Simulation. *Sustainability* **2024**, *16*, 7322. [CrossRef]
25. Zhou, Z.; Deng, J.; Wang, P.; Zhou, C.; Xu, Y.; Jiang, W.; Ma, K. Physical Environment Study of Traditional Village Patterns in Jinxi County, Jiangxi Province Based on CFD Simulation. *Processes* **2022**, *10*, 2453. [CrossRef]
26. Jun, Y.; Fu, L. Study on Wind Environment Simulation of Traditional Large Houses in Northeast Hunan. *Urban Archit.* **2021**, *18*, 126–129.
27. Wang, Y.; Wang, Y. Research on the Layout Design of Teaching Clusters in Lingnan Universities Based on Wind Environment Optimization. *Build. Energy Effic.* **2024**, *52*, 151–160.
28. Liu, T.; Huang, T.; Yang, H.; Wang, Y.; Wang, Z.; Chi, H.; Yu, X.; Xu, J.; Chen, J. Evaluation of the Influence of Outdoor Enclosed Space Facade Layout on Wind Comfort at the World Heritage Site. *Buildings* **2025**, *15*, 1451. [CrossRef]
29. Zhao, Z.; Zhang, S.; Peng, Y. Ecological Wisdom in Architectural Heritage: Taking the Wind Environment of the Bailudong Academy Complex as an Example. *South Archit.* **2023**, *12*, 49–57.
30. Liu, B.; Song, W.; Liu, Y.; Wang, C.; Song, J. Optimal Spatial Configuration for Energy and Solar Use in Alpine-Frigid Resettlement Communities. *Buildings* **2025**, *15*, 2691. [CrossRef]
31. Wan, F.; Li, Z.; Li, H.; Li, L.; Xiao, X. Climate-Adaptive Archetypes of Vernacular Villages and Their Application in Public Building Design: A Case Study of a Visitor Center in Chaoshan, China. *Buildings* **2025**, *15*, 2848. [CrossRef]
32. *GB 50176-2016*; Thermal Design Code for Civil Building. China Architecture & Building Press: Beijing, China, 2016.
33. Guo, W.; Yao, Y.; Wu, J.; Xu, W. Analysis of Near-Surface Wind in Jinhua City. *Zhejiang Meteorol. Sci. Technol.* **1993**, *4*, 24–25+14. [CrossRef]
34. Lou, J.; Wang, K.; Zhang, X.; Fan, Y.; Wang, Y. Analysis of Climate Change Characteristics and Identification of Extreme Climate-Sensitive Areas in Jinhua Region. *Desert Oasis Meteorol.* **2024**, *18*, 126–133.
35. Hong, T. *Ming and Qing Residential Buildings in Dongyang*; Tongji University Press: Shanghai, China, 2000.
36. *GB/T 50378-2019*; Assessment Standard for Green Buildings. China Architecture & Building Press: Beijing, China, 2019.
37. *DB11/938-2012*; Design Standard of Green Building. China Architecture & Building Press: Beijing, China, 2013.

Disclaimer/Publisher's Note: The statements, opinions and data contained in all publications are solely those of the individual author(s) and contributor(s) and not of MDPI and/or the editor(s). MDPI and/or the editor(s) disclaim responsibility for any injury to people or property resulting from any ideas, methods, instructions or products referred to in the content.